

Smart Sensing and Communication Co-Design for IIoT-Based Control Systems

Ruijie Fu^{ID}, Jintao Chen^{ID}, Yutong Lin^{ID}, An Zou^{ID}, Member, IEEE, Cailian Chen^{ID}, Member, IEEE, Xinping Guan^{ID}, Fellow, IEEE, and Yehan Ma^{ID}, Member, IEEE

Abstract—Industrial Internet of Things (IIoT)-based control is growing rapidly, such as smart factories and industrial automation. Sensing and transmitting physical state measurements is the first step and the prerequisite for IIoT-based control. However, sensor interference (e.g., electromagnetic interference on sensing, temperature, and humidity variations in the field) and network interference (e.g., metal obstacles and background noises) may destroy the control performance by interfering with sensing and communication processes. Most of the present upstream “fixed sensors-networking-state estimation” approaches cannot effectively deal with sensor and network interferences due to the fixed measurements/estimation and network resource limitations. To optimize the performance of IIoT-based control, we propose a smart sensing and communication co-design (SSCC) framework to select more potential sensors and establish the corresponding network scheduling. SSCC consists of a smart estimator (SE) and a sensing communication mode switching (SCMS) agent. The SE detects sensor interference and obtains resilient state estimation based on collaborative sensing. SCMS agent dynamically switches sensor selections and network configurations (routing and transmission number) in an integrated manner based on the network and plant states by solving a performance optimization problem. We propose a lightweight SCMS approach by searching a predefined mode table. We perform simulations integrating TOSSIM and MATLAB/Simulink, and semi-physical experiments on a real wireless sensor-actuator network composed of TelosB nodes. The results show that the SSCC framework can effectively improve the control performance and enhance network energy efficiency under various types of interference by dynamically selecting sensors and allocating network resources.

Index Terms—Industrial Internet of Things (IIoT)-based control, sensing and communication co-design, state estimation.

Manuscript received 23 January 2023; revised 10 June 2023; accepted 14 July 2023. Date of publication 3 August 2023; date of current version 24 January 2024. This work was supported in part by the NSF of China under Grant 62103268, Grant 92167205, Grant 62202287, Grant 61933009, and Grant 62025305; and in part by Shanghai Chenguang Program under Grant 21CGA11. (*Corresponding author: Yehan Ma*)

Ruijie Fu, Jintao Chen, Yutong Lin, and Yehan Ma are with the School of Electronic Information and Electrical Engineering, Shanghai Jiao Tong University, Shanghai 200240, China (e-mail: furj2022@sjtu.edu.cn; kiboik@sjtu.edu.cn; sobremesa@sjtu.edu.cn; yehanma@sjtu.edu.cn).

An Zou is with the UM-SJTU Joint Institute, Shanghai Jiao Tong University, Shanghai 200240, China (e-mail: an.zou@sjtu.edu.cn).

Cailian Chen and Xinping Guan are with the Department of Automation and the Key Laboratory of System Control and Information Processing, Ministry of Education of China, Shanghai Jiao Tong University, Shanghai 200240, China (e-mail: cailianchen@sjtu.edu.cn; xpguan@sjtu.edu.cn).

Digital Object Identifier 10.1109/JIOT.2023.3299632

I. INTRODUCTION

WITH the development of embedded intelligence and the Industrial Internet of Things (IIoT), IIoT-based control is playing the leading role in the fourth industrial revolution [1], [2]. Recent advances in sensing, wireless networks, computing, and control are changing the way control systems interact with cyber and physical processes [3]. Industrial wireless networked control systems (WNCSs) based on IIoT integrate designs of computing, communication, and physical systems, which can make the system more reliable, efficient, and collaborative and have essential and broad application prospects. Owing to the rapid development of wireless technologies, WNCSs are no longer limited to only transmitting the measurements from sensors to the controller but also try to replace the traditional wired connections between controllers and actuators because of the high flexibility and less deployment and maintenance cost. The specific industrial network is called the wireless sensor and actuator network (WSAN). Nowadays, some industry standards and their applications in industrial automation [4], [5] have witnessed the great success of WSAN.

Sensing and communication are two of the critical processes of a cyber–physical system. In IIoT-based control systems, sensing and transmitting physical state measurements are the prerequisite for the control and actuation of the physical plants. The reliability and efficiency of sensing and communication directly dominate the control performance. However, IIoT-based control may suffer from sensor interference (electromagnetic interference [6], temperature and humidity variations [7], etc.) and network interference (background noises, metal obstacles [4], etc.) subjected to limited sensing and communication resources in the industrial field, resulting in deteriorated control performance caused by the reduction of the reliability and efficiency for sensing and communication.

Transmission of measurements of the industrial plants from fixed sets of sensors via WSAN to resilient state observers [8], [9], [10] is a common approach in IIoT-based control systems. However, the interference on critical sensors or the network links may directly affect the observation performance and destroy the control performance. Intuitively, the adverse impacts of interference could be eliminated by introducing redundancy of sensing and communication. However, a casual redundancy of sensors and their corresponding wireless configurations may have limited improvements in observation and control performance due to the limited sensing and communication resources.

Regarding sensor and network interferences, most research results tend to design solutions for a specific type of interference from the perspective of state estimation or networking, such as the anti-outliers Kalman filter (KF) [11], which detects and adapts to measurement outliers. The dynamic adaptive routing protocol [12], [13] guarantees communication performance when the wireless network changes, etc. However, the separated solutions for sensor or network interference do not consider the deep integration between sensing and communication. For example, if a sensor is malfunctioning, continuing to ensure reliable transmission of anomalous measurements is a waste of network resources. Likewise, the more unreliable the wireless link is, the more probability the measurement would be interfered due to the binary transmission. Furthermore, the allocation of sensing and communication resources should be adjusted as the dynamics and kinematics of the industrial plants evolve. Therefore, the co-design of sensing and communication is essential to improve the overall performance of the IIoT-based control system. The key challenges for co-designing sensing and communication are how to effectively integrate advanced sensing and communication technologies and how to balance the trade-off between limited sensing and network resources, and the resiliency and control performance requirements.

Contribution: In this work, we propose a smart sensing and communication co-design (SSCC) framework for IIoT-based control systems, overcoming the sensor and network interferences in an integrated manner at run-time. First, potential sensors measuring different plant states are selected for WNCS based on a smart estimator (SE) which coordinates a series of state observers for sensor interference detection and reliable state estimation. Second, the sensing and communication mode switching (SCMS) agent is introduced, which dynamically selects sensors and configures the network (routing and transmission number) based on the status of sensor and network and evolution of physical plants. The SSCC can optimize the overall performance subjected to limited sensing and communication resources, even facing sensor and network interference. Our major contributions are fourfold.

- 1) An SSCC framework for IIoT-based control systems is proposed to optimize the overall control performance of multiple control loops subjected to limited resources, facing both sensor and network interferences. In this framework, SSCC deploys multiple heterogeneous sensors measuring different physical states and divides them into three categories: a) main sensors; b) auxiliary sensors; and c) anomaly sensors. To detect the anomaly in time while saving the network cost, a dual-time sensing-communication (SC) scheduling is used to transmit the sensor measurements to the remote controller.
- 2) We design a SE which diagnoses sensor interference and process disturbance based on a self-diagnose and the collaboration of multiple sensors. A smart KF, which integrates two intermittent KF submodules, called primary KF and adjoint KF, can estimate physical states under the dual-time scheduling reliably. Such a scheduling can be robust to the network interference by dynamically allocating the constrained network resource of the small

timescale while conducting the sensor anomaly detection by more sensor candidates efficiently in the large timescale.

- 3) An SCMS agent is presented for dynamic switching of SC mode based on network conditions, sensor interference, and the evolution of the physical states. We formulate the SC co-design optimization problem as a *multiobjective optimization problem* for minimizing the state estimation error, network transmission cost, and reconfiguration cost. A lightweight heuristic approach by searching a predesigned SC mode table is proposed for SC mode selection.
- 4) The SSCC framework is implemented on a high-fidelity TOSSIM simulation environment and semi-physical experiments on a WSAN composed of TelosB nodes. Extensive evaluations and a state-of-art comparison demonstrate the efficacy of SSCC under fluctuating sensing and network conditions.

Organization: The remainder of this article is organized as follows. Section II reviews related works. Section III overviews SSCC framework. Section IV introduces the SE. Section V details the SSCC approach and the design of SCMS Agent. Section VI evaluates the simulation and experiment results. And we present our conclusions in Section VII.

Notation: The notation used in this article is mostly standard. \mathbb{N} is the set of natural numbers. \mathbb{R}^n is the n -dimensional Euclidean space. $\mathbb{R}^{m \times n}$ is a set of all $(m \times n)$ real matrices. A^T , A^{-1} , $\text{Tr}(A)$, $\rho(A)$, and $\text{diag}(A)$ the transpose, the inverse, the trace, the spectral radius of the matrix A , and the column vector consisting of the diagonal elements of the matrix A , respectively. $x \sim \mathcal{N}(\mu, W)$ represents a multivariate Gaussian distributed random vector x with mean vector μ and positive-definite covariance $W > 0$. We denote expectation and conditional expectation by $\mathbb{E}[\cdot]$ and $\mathbb{E}[\cdot | \cdot]$, respectively. e_i is the basic column vector with the i th component as 1, e.g., $e_2 = [0, 1, \dots, 0, \dots, 0]$. $\mathbb{1}(\cdot)$ is the indicator function, if the condition in (\cdot) is true, $\mathbb{1}(\cdot) = 1$, if false, $\mathbb{1}(\cdot) = 0$. \neg is the logical NOT operator. For a finite set S , we employ $|S|$ to denote its cardinality, i.e., the number of elements in S . $\|x\|_\infty$ denotes the l_∞ -norm which is defined as $\|x\|_\infty = \max_{1 \leq j \leq n} |x_j|$. Table I summarizes the key notations and abbreviations used in this article.

II. RELATED WORK

In this section, we first review the state-of-the-art estimation and networking approaches overcoming sensor and wireless network interference. Then we study the researches to detect sensor anomalies in wireless sensor networks. Finally, we investigate the studies of sensing, networking, and control co-design approaches in IIoT-based control.

Different state estimation approaches have been investigated for sensing anomalies in the WNCS architecture of fixed sensors and state observers. Fisch et al. [14] developed a particle and outlier robust filter by combining Rao–Blackwellisation and well-designed proposal distributions. Chernikova [15] introduced an algorithm for handling anomalous measurements with an adaptive unscented KF.

TABLE I
NOTATIONS AND ABBREVIATIONS

Symbols	Interpretation	Symbols	Interpretation
SSCC	Smart Sensing and Communication Co-design	LMRLS	Limit Memory Recursive Least Square algorithm
SE	Smart Estimator	SCMS	Sensing-Communication Mode Switching
KF	Kalman Filter	PDR	Packet Delivery Radio
T_s	the sampling period	s_n	the main sensor of loop n
T_c	the coordination period, $T_c = H * T_s$	$\hat{x}_{main,n,t}$	the state estimation by $KF_{m,n}$ of s_n in loop n ($\hat{x}'_{main,n,t}$ by $KF'_{m,n}$)
$KF_{m,n}$	the primary KF of sensor m in loop n	$NS_{n,t}$	the normal sensor set of loop n
$KF'_{m,n}$	the adjoint KF of sensor m in loop n	$IS_{n,t}$	the anomaly sensor set of loop n
Q_n	the covariance matrix of the process noise in loop n	$\bar{x}_{n,t}$	the final estimation result by SE of loop n
$R_{m,n}$	the covariance of the measurement noise of sensor m in loop n	$\hat{\theta}_{n,t}$	the parameter identification result of LMRLS
$\hat{y}_{m,n,t}$	the measurement of sensor m in loop n	$K_{n,t}$	the gain matrix of LMRLS
$\varphi_{m,n,t}$	the binary bit which represents the packets reception ($\varphi_{m,n,t} = 1$) or loss ($\varphi_{m,n,t} = 0$) for sensor m in loop n	$P_{n,t}$	the error covariance matrix of LMRLS
$\hat{x}_{m,n,t}$	the state prediction of $KF_{m,n}$ ($\hat{x}'_{m,n,t}$ in $KF'_{m,n}$)	$h_{n,t}$	the measurement data vector of LMRLS
$P_{m,n,t}^-$	the error covariance matrix between $x_{n,t}$ and $\hat{x}_{m,n,t}$ ($P'_{m,n,t}$ in $KF'_{m,n}$)	$\hat{\Theta}_{n,t}$	the estimated parameters of LMRLS
$K_{m,n,t}$	the Kalman gain of $KF_{m,n}$ ($K'_{m,n,t}$ in $KF'_{m,n}$)	R_n	the routing for s_n of loop n
$\hat{x}_{m,n,t}$	the state estimation of $KF_{m,n}$ by $\hat{y}_{m,n,t}$ or $\bar{y}_{m,n,t}$ ($\hat{x}'_{m,n,t}$ in $KF'_{m,n}$)	η_n	the transmission scheduling for s_n of loop n
$P_{m,n,t}$	the error covariance matrix between $x_{n,t}$ and $\hat{x}_{m,n,t}$ ($P'_{m,n,t}$ in $KF'_{m,n}$)	$p(s_n, R_n, \eta_n)$	the estimated PDR under s_n , R_n , and η_n
$\bar{\lambda}_n$	the bound of PDR to guarantee the convergence of $P_{m,n,t}$	$V_{n,t}$	the value of the Lyapunov function of loop n
$TH_{m,n,t}^\pm$	the boundary of the normal range for $\hat{x}_{m,n,t}$	L_{frame}	the total slot number of a superframe
$\tilde{x}_{n,t}^{\pm Q}$	the process estimation under the maximal state noise $\pm \sqrt{\text{diag}(Q_n)}$	$e_{n,t}$	the estimation error between $x_{n,t}$ and $\bar{x}_{n,t}$
$\tilde{y}_{m,n,t}^{\pm Q}$	the measurement extracted from $\tilde{x}_{n,t}^{\pm Q}$	$PRR_{R_n,h}$	the packet delivery radio in the h -th link in R_n
$\tilde{y}_{m,n,t}^{\pm R}$	the measurement with the noise $\pm \sqrt{R_{m,n}}$ adding to $\tilde{y}_{m,n,t}^{\pm Q}$	S	the overall SC mode combined N loops' S_n
$\hat{x}_{m,n,t}^{\pm R}$	the state estimation using the $\tilde{y}_{m,n,t}^{\pm R}$	δ	the number of update slots between two different S
$I_{m,n,t}$	the binary bit which represents the anomaly ($I_{m,n,t} = 1$) or normal ($I_{m,n,t} = 0$) state of sensor m in loop n	S_n	the SC mode of loop n consists of s_n , R_n , and η_n
$\bar{y}_{m,n,t}$	the measurement of sensor m extracted from $\bar{x}_{n,t}$ for collaborative KF updating	hop_{R_n}	the total hop count of R_n

Wang et al. [16] proposed a state-estimation method based on an intermittent KF and the Gaussian mixture reduction to process time-varying and featureless sensor faults. Fang et al. [17] developed an innovation-saturated EKF (ISEKF), which can adaptively adjust the innovation saturation bounds to reject outliers. For multiple sensors environment, distributed estimation provides a fault-robust fusion framework with a peer-to-peer communication architecture. It effectively improves robustness to sensor interference by designing sensors' adaptive KF algorithm [18], [19], [20]. Physical plants can deviate from their state trajectory during operation due to unexpected external disturbance called process disturbance. Process disturbance also causes the abnormality of sensor measurements, which, however, does not indicate that the sensor is malfunctioning. These works effectively solve the sensor interference associated with anomalous measurements, but most of them do not consider the process disturbance, which may frequently appear, and distinguish it from the sensor interference. Moreover, they are not resilient to network environment changes and packet loss [21] by assuming perfect connections between sensors and estimators. However, this assumption is not realistic in harsh industrial wireless networks.

Therefore, a number of estimation and filtering approaches have been developed for sensing packet loss and delay

in wireless networks under specific network packet loss models [22], [23], [24]. However, most of the studies treat the network as a transient medium with loss and delay while ignoring the reconfigurability of the wireless network. Actually, by designing dynamic configuration strategies for wireless networks, the changes in the network environment can be effectively addressed, which can realize the effective allocation of network resources and reliable communication. An optimal GTS allocation mechanism is proposed in accordance with the data requirements of the nodes [25]. The packet retransmission counts [26], channel selection [27], routing [28], and reachability-aware scheduling [29] can effectively improve the packet delivery rate (PDR) of measurements when the network changes or interference happens. Most of the above works model the message dropout as a Bernoulli random process, but these studies assume the perfect sensor measurements and do not consider the content of the packet and the various demands on network resources as the physical plants evolve. As a result, those approaches of network resource allocation cannot optimize the performance of the control system based on physical dynamics.

Different frameworks for detecting interference have been extensively studied. For sensors fault detection, Yemeni et al. [30] presented a centralized faulty data detection and recovery (CFDDR) approach, which can recognize

different types of faults and replace the faulty data by an estimated value based on the KF. Although CFDDR is efficient and accurate, every sensor node in WSN reports periodically to the centralized node to check whether they are faulty or not, thus lead to extra network costs. Sharma and Sharma [31] proposed a reactive distributed fault detection (rDFD) to detect faulty data. However, if the fault rate is high, the network cost will be high since the nodes need to exchange data with their neighbors frequently [30]. Although those works receive accurate detection results, they ignore the design freedom of the network scheduling for each sensor and thus increase the energy consumption of the entire wireless work. Moreover, scheduling is especially critical when network interference happens while the sensors may not guarantee their measurements to be delivered. In such a situation, the detection accuracy will also be affected not matter how accurate the sensor anomaly detection is.

There has been many works on the co-design of networks with control or observation. Lu et al. [1] explained the concept of cyber–physical co-design. Li et al. [32] improved resource utilization by investigating the scheduling of emergency and regular flows in WirelessHART networks. Ma et al. [33] dynamically configured the WSAN by designing a holistic architecture to maintain the required control performance while saving wireless resources. By using information from both the physical plants and the wireless network, it is evident that the strategy of cyber and physical co-design can effectively improve control performance. Li et al. [34] proposed a transmission power scheduling online of a fixed sensor to carry out remote state estimation. Ding et al. [35] proposed a multichannel transmission schedule for remote state estimation under DoS attacks. Although some existing studies deploy the intermittent KF or configure the scheduling (e.g., routing and transmission) to deal with network interference, most of those works apply fixed sensors. As a result, they are less robust to sensor interference such as incorrect measurements. As the co-design approach can improve the observation/control performance and enhance the network efficiency, this inspires us to leverage the co-design approach to jointly deal with sensor interference and network interference. To the best of our knowledge, Ma et al. [36] considered the observation by formulating the sensor scheduling problem with an imperfect sensor into a finite-dimensional MDP. However, this work assumes a static network condition and does not consider the sensor measurement bias or noise distribution change. In this work, we will propose a prototype for smart sensor selection and communication co-design under varying sensor and network interferences.

III. SSCC FRAMEWORK AND MODELS

A. Backgrounds of the IIoT-Based Control System

An IIoT-based control system with N closed loops is shown in Fig. 1. Each loop includes a physical plant, sensors, a state observer, a controller, an actuator, and the wireless network shared with other loops. The sensors measure the physical states y_t of the industrial plant and transmit it to the observer via the wireless network. The observer calculates the full state

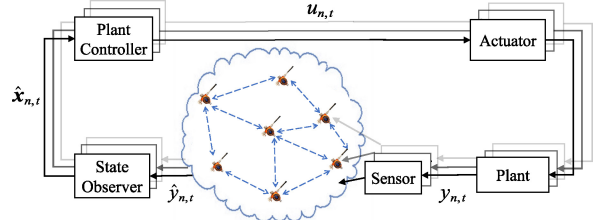


Fig. 1. IIoT-based control system architecture.

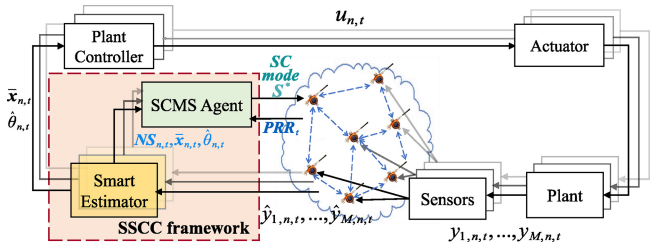


Fig. 2. SSCC framework in IIoT-based control.

estimation \hat{x}_t , and the controller establishes the actuation command u_t based on \hat{x}_t and sends u_t to the actuator. As we are targeting the design of sensing and uplink communication in this work, for simplicity, we assume a wired connection between the controller and the actuator [37], [38], [39].

For the n th loop, the corresponding plant is modeled as a discrete-time linear time-invariant (DT-LTI) system

$$x_{n,t} = A_n x_{n,t-1} + B_n u_{n,t-1} + w_{n,t-1} \quad (1)$$

$$y_{n,t} = C_n x_{n,t} + v_{n,t} \quad (2)$$

where t is the time index, n is the loop index, $x_{n,t} \in \mathbb{R}^a$ is the state vector, and $u_{n,t} \in \mathbb{R}^b$ is the input vector. For state estimation, the intermittent KF [40] applicable to the packet delay and loss in wireless networks is applied, which is detailed in Section III-C3. For the controller, we adopt the classical feedback control model, i.e., $u_{n,t} = g_n(x_{n,t})$, where $g_n(\cdot)$ is the control law, $y_{n,t} \in \mathbb{R}^c$ is the output vector, $A_n \in \mathbb{R}^{a \times a}$, $B_n \in \mathbb{R}^{a \times b}$, and $C_n \in \mathbb{R}^{c \times a}$. $w_{n,t} \in \mathbb{R}^a$ and $v_{n,t} \in \mathbb{R}^c$ are Gaussian noise with zero mean and covariance $Q_n \succeq 0$ and $R_n > 0$, respectively. We assume that the pair (A_n, B_n) is controllable.

B. SSCC Framework

The IIoT-based control system with our SSCC framework is shown in Fig. 2, which includes multiple potential sensor choices. SSCC comprises two advanced modules: 1) SE and 2) SCMS Agent. We come up with the SE that can detect and distinguish the interference in sensors and the process disturbance in industrial plants and select normal sensors based on different state measurements and the coordination of a series of corresponding state observers within the SE. To cope with the impact of changes in model parameters, SE also integrates a dynamic identification algorithm for physical parameters. We will introduce the SE in detail in Section IV.

Although the SE can select sensor candidates without interference, it cannot allocate limited network resources according to the changing network condition and the varying

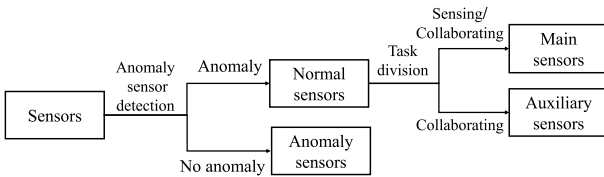


Fig. 3. Sensor categories.

network demands of industrial plants. To solve this problem, we propose an SCMS Agent, which dynamically selects sensors and configures the wireless network for selected sensors, according to sensor candidates provided by SE, physical and network states. In this way, the overall control performance of multiple control loops can be optimized. We will introduce the SCMS module in detail in Section V.

C. Sensing and Estimation

1) *Sensing*: The proliferation of low-cost, lightweight, and power-efficient sensors and wireless networks enables the employment of a large amount of sensors [41]. We classify the tasks of sensors in WSAN into two types and divide all sensors into three categories based on their interference status and the tasks they execute as shown in Fig. 3. The first type of task is *sensing*, in which the measurements achieved by sensors are transmitted to the state observer to obtain full state estimation. As transmitting all the measurements at one time consumes a large amount of network resources, inspired by the Health Reports mechanism of the wirelessHART [42], where the device periodically communicates with the network manager (NM) to report its conditions, we consider collaborating as another task. Sensors with collaborating task transmit their measurements to detect sensor interference collaboratively in a longer period than the normal sampling period, which we will explain amply in Section III-C2. We divide sensors into three categories: 1) *main sensors*, which operate sensing tasks without sensor interference under relatively good network conditions; 2) *auxiliary sensors*, which participate in collaborating tasks without sensor interference under relatively good network conditions; and 3) *anomaly sensors*, which are detected sensor interference.

State estimation, such as the intermittent KF described in Section III-C3, assumes the detectability of the pair (C_n, A_n) in (1). Detectability is a prerequisite for reconstructing state estimations from measurements [43]. Since the deployment of sensors determines the form of the matrix C_n , it should satisfy the detectability. In addition, the selection of candidate sensors should take the practical knowledge of possible interferences and network capacities into consideration.

2) *Dual-Timescale Sensing and Communication*: The deployment of an excess amount of sensors gains resiliency to sensor interference at the cost of network resources to transmit $y_{n,t}$. To reconcile the conflict between the network efficiency and the observation performance of the system, we propose a dual-timescale SC co-design strategy, given the tasks of sensors in WSAN and sensor categories described in Section III-C1), which will be overviewed in the following and detailed in Section V.

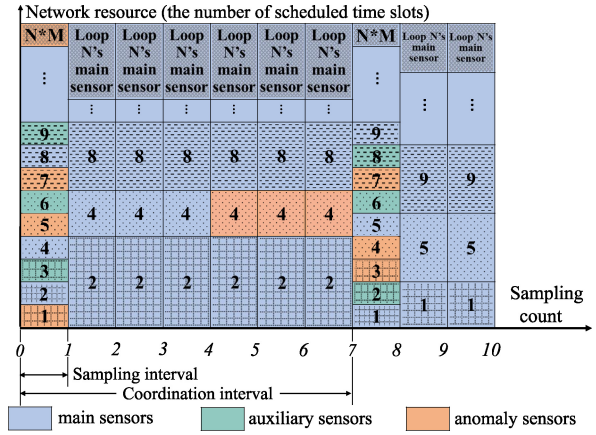


Fig. 4. Dual-timescale SC co-design.

In large timescale, we define the coordination period T_c , which is multiples of the sampling period T_s , i.e., $T_c = H * T_s$, where $H \in \mathbb{N}$. At the beginning of T_c , sensor candidates collaborate to detect sensor interference with the help of the SE, and the SCMS agent updates main sensor selections and network configurations, such as routing and retransmissions. In small timescale T_s , the main sensors transmit measurement to the SE with fixed network configuration determined in the large timescale to get full state estimation and run-time sensor interference self-detection.

Fig. 4 shows an example of dual-timescale SC co-design. The x -axis is the sampling counts, which is a normalization form of the sampling period by ignoring the scheduling within each period. The y -axis is the network resource allocation (number of time slots) for the delivery of each sensor measurement. The height of a rectangle indicates the number of time slots allocated to a certain sensor measurement. The physical state is measured by the sensor with an index in the middle of each rectangle. And all the rectangles in the same column represent the resultant resource allocation to deliver sensor measurements in one sampling period. Different background colors denote the types of sensors (main, auxiliary, and anomaly sensors). With $H = 7$, at sampling counts 0, 7, etc., the SCMS agent schedules the transmissions of candidate sensors, and at sampling counts 1 to 6, only main sensors (2, 4, 8, etc.) are scheduled to transmit at proper network resource cost determined by the SCMS Agent. At those sampling periods, there are 4, 2, and 3 time slots scheduled for delivering the measurements of sensors 2, 4, and 8, respectively. At sampling count 4, sensor 4 is detected to be abnormal by smart estimation in the small timescale. At sampling count 7, anomalies in sensors 3 and 7 are detected by collaboration, while anomalies for sensors 1 and 5 end. Main sensors at sampling counts 8 to 10 are sensors 1, 5, 9, etc.

Remark 1: The matrix C_n would change with the main sensor selection. Specifically, if the only main sensor measures the m th state in the state vector $x_{n,t}$, at that time, the matrix C_n can be denoted as a row vector which the m th bit is one while others are zero, i.e., $C_n = e_m^T$. For example, if the main sensor 1 measure x_1 , then the output matrix is changed to $C_n = e_1^T = [1 \ 0 \ 0]$.

3) *Estimation*: The state estimation process of the intermittent KF consists of two steps: 1) *predict* and 2) *update*. The update step is modified when packets are dropped by the wireless network. The intermittent KF for the single sensor m of the control loop n [40] is shown in

$$\hat{x}_{m,n,t}^- = A_n \hat{x}_{m,n,t-1} + B_n u_{n,t-1} \quad (3)$$

$$P_{m,n,t}^- = A_n P_{m,n,t-1} A_n^T + Q_n \quad (4)$$

$$K_{m,n,t} = P_{m,n,t}^- C_n^T (C_n P_{m,n,t}^- C_n^T + R_{m,n})^{-1} \quad (5)$$

$$\hat{x}_{m,n,t} = \hat{x}_{m,n,t}^- + \varphi_{m,n,t} K_{m,n,t} (y_{m,n,t} - C_n \hat{x}_{m,n,t}^-) \quad (6)$$

$$P_{m,n,t} = P_{m,n,t}^- - \varphi_{m,n,t} K_{m,n,t} C_n P_{m,n,t}^- \quad (7)$$

where $\hat{x}_{m,n,t}^-$ denotes the predicted value of the state by $\hat{x}_{m,n,t-1}$ and $u_{n,t-1}$, C_n is the output matrix in (1) associated with the $y_{m,n,t}$, $P_{m,n,t}^-$ is the error covariance matrix between the real plant state $x_{n,t}$ and $\hat{x}_{m,n,t}$, $K_{m,n,t}$ is the Kalman gain, $\hat{x}_{m,n,t}$ is the estimation of the state, $P_{m,n,t}$ is the error covariance matrix between $x_{n,t}$ and $\hat{x}_{m,n,t}$, and the binary variable $\varphi_{m,n,t}$ represents the successful reception ($\varphi_{m,n,t} = 1$) or loss ($\varphi_{m,n,t} = 0$) of the measurement $y_{m,n,t}$ transmitted through WSAN at time t . If $\varphi_{m,n,t} = 1$, $\hat{x}_{m,n,t}$ is equal to the state prediction $\hat{x}_{m,n,t}^-$ plus a correction item based on $y_{m,n,t}$. If $\varphi_{m,n,t} = 0$, $\hat{x}_{m,n,t}$ is equal to the state prediction $\hat{x}_{m,n,t}^-$. In this article, we assume $y_{m,n,t}$ to be scalar measurements for simplicity, which has been used in many designs of wireless network control systems [34], [44], [45] and distributed multisensor fusion [41], and the case of multidimensional $\hat{y}_{n,t}$ will be discussed in our future work.

There is a critical bound $\bar{\lambda}_n$ of PDR to guarantee the statistical convergence of $P_{m,n,t}$ [40], [46], which is derived by solving a quasi-convex optimization problem [40, Corollary 1]. Therefore, if a certain wireless network configuration cannot guarantee the prerequisite of filter convergence (i.e., PDR is smaller than $\bar{\lambda}_n$), SCMS agent should update SC mode with a higher PDR, if possible, for convergent state estimation.

D. Wireless Network

1) *IEEE 802.15.4 Superframe*: We apply the wireless network based on the IEEE 802.15.4 standard for sensing and communication co-design. The IEEE 802.15.4 standard has been the most frequently adopted communication standard for WNCS [3] and is widely applied in industrial control. A superframe is a collection of timeslots that repeat in time. In beacon-enabled mode, the beacon frame transmission starts at the beginning of the first slot of each superframe. Beacons that are sent by the coordinator node are used to synchronize connected devices, identify the network and describe the structure of the superframe. During the inactive period, the wireless nodes enter a low-power mode. The active period consists of contention access period (CAP) and contention free period (CFP). During the CAP, the device competes for media access using a carrier listening multiple access/collision avoidance (CSMA/CA) MAC scheme. For applications with real-time performance requirements, the NM provides GTS exclusively during the CFP. The number of time slots allocated to the CAP and CFP could be a free design parameter in the modification [47]. In this article, we target IIoT-based

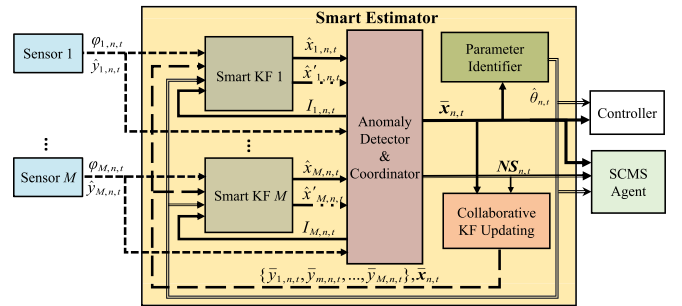


Fig. 5. SE architecture.

control systems with real-time performance requirements by placing the superframe scheduling of all sensors on the CFP.

2) *Network Reconfiguration*: The NM manages the network and its wireless nodes. The NM, the plant controller, and the coordinator of the network are usually in the same place or connected via a reliable wired network with negligible packet drop and latency [48], [49]. While we deploy SCMS agent directly into NM, after receiving the updated SC mode from the NM, the coordinator broadcasts the schedule by the beacon frame at the beginning of the next superframe. In this way, nodes that receive the beacon update their schedules.

IV. SMART ESTIMATOR

A. Smart Estimation Architecture

Fig. 5 overviews the architecture of SE for loop n , which integrates an anomaly detector and coordinator to detect sensor interference, a collaborative KF updating module to stimulate the KF of auxiliary sensors, and a parameter identifier (PI) for dynamic identification of physical parameters. The inputs of the SE are the measurement sets $\hat{y}_c = \{\hat{y}_{1,n,t}, \dots, \hat{y}_{M,n,t}, \dots, \hat{y}_{M,n,t}\}$ and the packet reception status $\varphi_c = \{\varphi_{1,n,t}, \dots, \varphi_{M,n,t}, \dots, \varphi_{M,n,t}\}$ of candidate sensors at the beginning of T_c , where M is the total number of candidate sensors. Each sensor has a corresponding smart KF, which obtains the state estimation $\hat{x}_{m,n,t}$. The anomaly detector and coordinator detects sensor interference through the dynamic normal state estimation ranges and sensor collaboration by state estimation sets $\hat{x}_c = \{\hat{x}_{1,n,t}, \dots, \hat{x}_{m,n,t}, \dots, \hat{x}_{M,n,t}\}$, and generates the anomaly detection results $I_{m,n,t}$ in each sampling period T_s to the smart KF, and the normal sensor selection results $NS_{n,t}$ at large timescale to the collaboration KF updating and SCMS Agent. A final state estimation $\bar{x}_{n,t}$ is selected by anomaly detector and coordinator to transmit into the PI, collaborative KF updating, SCMS Agent, and controllers. The PI calculates the model parameter estimation result $\hat{\theta}_{n,t}$ of real plant parameters $\theta_{n,t}$, and sends $\hat{\theta}_{n,t}$ to controllers, all smart KFs, and SCMS Agent. The collaborative KF updating module generates the estimated $\bar{y}_{n,t}$ and $\bar{x}_{n,t}$ to stimulate KFs of auxiliary sensors in each sampling period T_s .

B. Smart Kalman Filter

As shown in Fig. 6, each sensor has a corresponding smart KF, which includes two submodules and obtains two sets

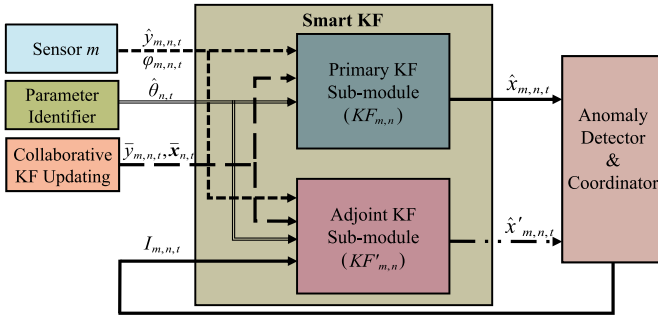


Fig. 6. Smart KF structure.

of state estimations $\hat{x}_{m,n,t}$ and $\hat{x}'_{m,n,t}$ by the primary KF and adjoint KF, respectively. In large timescale (the first T_s in T_c), the smart KF collects and updates the information of measurement $\hat{y}_{m,n,t}$, the packet reception status $\varphi_{m,n,t}$, the parameter identification result $\hat{\theta}_{n,t}$, and the results of sensor m 's anomaly detection $I_{m,n,t}$. In small timescale (each T_s except the first one within T_c), the smart KF collects measurement $\hat{y}_{m,n,t}$ if sensor m is the main sensor, or the stimulated measurements $\bar{y}_{m,n,t}$ from the collaboration KF updating module otherwise.

Let $\mathbf{IS}_{n,t}$ be the set of abnormal sensors ($I_{m,n,t} = 1$), and $\mathbf{NS}_{n,t}$ be the set of normal sensors ($I_{m,n,t} = 0$). The $\mathbf{IS}_{n,t}$ and $\mathbf{NS}_{n,t}$ are updated according to $I_{m,n,t}$ in each large timescale. In large timescale (the first T_s of T_c), the *primary KF* ($KF_{m,n}$) derives state estimation $\hat{x}_{m,n,t}$ based on $\hat{y}_{m,n,t}$ or $\bar{y}_{m,n,t}$ (detailed in Section IV-C3) according to (3)–(7). In small timescale (each T_s except the first one in T_c), if $m \in \mathbf{NS}_{n,t}$ or m is the main sensor, the primary KF follows the above procedures, and if $m \in \mathbf{IS}_{n,t}$, the primary KF modifies (6) as

$$\hat{x}_{m,n,t} = \hat{x}_{m,n,t}^- \quad (8)$$

Our rationale is as follows. If main sensor anomaly is detected, i.e., $I_{m,n,t} = 1$, the auxiliary sensors' primary KFs only operate the prediction step for in Section IV-C2. At each T_s , *adjoint KF* ($KF'_{m,n}$) always applies (9) instead of (6)

$$\begin{aligned} \hat{x}'_{m,n,t} &= \hat{x}'_{m,n,t}^- \\ &+ K'_{m,n,t}(1 - I_{m,n,t})\varphi_{m,n,t}(y_{m,n,t} - C_n \hat{x}_{m,n,t}^-). \end{aligned} \quad (9)$$

As a result, if sensor anomaly is at time t_a , i.e., $I_{m,n,t} = 1$, adjoint KF does not estimate based on the abnormal \hat{y}_{m,n,t_a} as the primary KF. Instead, it operates prediction to achieve $\hat{x}'_{m,n,t}$ by setting $\hat{x}'_{m,n,t_a} = \hat{x}_{m,n,t_a}^-$ in (9) based on previous normal state estimation \hat{x}_{m,n,t_a-1} . That is, $\hat{x}'_{m,n,t_a} = A_n \hat{x}_{m,n,t_a-1} + B_n u_{n,t_a-1}$ at time t_a .

Regarding the status of packet reception, in large timescale, if sensor m successfully receives the packet, i.e., $\varphi_{m,n,t} = 1$, the smart KF applies $\hat{y}_{m,n,t}$ to update primary and adjoint KFs according to (6) and (9), respectively. If $\varphi_{m,n,t} = 0$, both primary and adjoint KFs only operate prediction according to equivalent (6) and (9) as the second terms are 0. In small timescale, the main sensor follows the above procedures for sensor m . For the auxiliary smart KF corresponding to auxiliary sensors that are not scheduled to work, $\bar{y}_{m,n,t}$ extracted from $\bar{x}_{n,t}$ is fed into both primary and adjoint KFs instead of

$\hat{y}_{m,n,t}$ for stimulating and synchronizing the KF calculation if the main sensor is no anomaly detected.

During the initialization, the two submodules are set to the same initial state $x_{n,0}$ as well as the initial error covariance matrix $P_{m,n,0}$. After detecting the recovery of the short-term sensor interference, we set the final estimation result $\bar{x}_{n,t}$ of the SE as the initial state value of the smart KFs, which we will detail in Section IV-C3.

In summary, applying both primary and adjoint KFs can realize a reliable state estimation and distinguish the process disturbance. When the main sensor is detected to be anomaly by $[TH_{m,n,t}^-, TH_{m,n,t}^+]$, the SE can use the adjoint KF's state prediction until the next large timescale. The primary KF still updates by the anomaly measurement $\hat{y}_{m,n,t}$ in order to distinguish the process disturbance from the sensor interference, which we will detail in Section IV-C2.

C. Anomaly Detector and Coordinator

1) *Anomaly Sensor Detection*: Measurement outliers would increase the state estimation error and further drive away the estimation at the next time instant, potentially leading to divergence. Therefore, the anomaly measurements should be discarded for state estimation [50]. Some probability-based policies are used to reject the outliers. In [51], the EKF detects an outlier by evaluating the probability of its occurrence based on innovation statistics. The measurement-weighting-based approach [52] assigns the measurement at each time with a weight and downweight the outlying measurement by iteration. However, some of them involve a significant increase in computational complexity due to iterative optimization or other computationally expensive procedures [17]. Meanwhile, some rejection thresholds which are widely applied in outlier-robust filtering are proposed to reject the outliers, such as the common 3σ threshold [53], the surprisal threshold [54], and the dynamic threshold [17], due to their less computational complexity. It is worth noting that since the purpose of our work is not to improve the accuracy of anomaly detection but to provide a control and communication co-design framework to deal with sensor and network interferences. Also, considering the need of WNCSSs for low-computational complexity at run-time, we apply the commonly used and mature 3σ thresholds as the criteria for sensor anomaly detection for simplicity.

According to the assumptions that $w_{n,t}$ and $v_{n,t}$ in (1) and (2) are mean-zero Gaussian noises, and we use $v_{m,n,t}$ instead of $v_{n,t}$ to denote the measurement noise of sensor m , we define $w_{n,t}$ and $v_{m,n,t}$ within the ranges of $[-3\sqrt{\text{diag } Q_n}, 3\sqrt{\text{diag } Q_n}]$, $[-3\sqrt{R_{m,n}}, 3\sqrt{R_{m,n}}]$, respectively, as normal based on 3σ criterion. Then we can get a dynamic range $[TH_{m,n,t}^-, TH_{m,n,t}^+]$ for the normal estimation of sensor m based on above normal ranges of noises, as time t passing by. If $\hat{x}_{m,n,t}$ exceeds this range, sensor m is labeled as anomaly.

When both $w_{n,t}$ and $v_{n,t}$ take their maximum normal values, we calculate the virtual sensor measurements $\tilde{y}_{m,n,t}^{*\pm R}$ in this case. Using $\tilde{y}_{m,n,t}^{*\pm R}$, $\bar{x}_{n,t-1}$ and the error covariance matrix

$P_{m,n,t-1}$ of the KF to estimate the normal state estimation range, the calculation steps are shown

$$\tilde{x}_{n,t}^{\pm Q} = A_n \bar{x}_{n,t-1} + B_n u_{n,t-1} \pm 3\sqrt{\text{diag}(Q_n)} \quad (10)$$

$$\tilde{y}_{m,n,t}^{\pm Q} = e_m^T \tilde{x}_{n,t}^{\pm Q} \quad (11)$$

$$\tilde{y}_{m,n,t}^{*\pm R} = \tilde{y}_{m,n,t}^{\pm Q} \pm 3\sqrt{R_{m,n}} \quad (12)$$

$$\hat{x}_{m,n,t}^{\pm R} = K F_{m,n}(\tilde{y}_{m,n,t}^{*\pm R}, \bar{x}_{n,t-1}, P_{m,n,t-1}) \quad (13)$$

where $\tilde{x}_{n,t}^{\pm Q}$ are state predictions under the maximum normal state noise $w_{n,t}$ at $\pm 3\sqrt{\text{diag}(Q_n)}$. $\tilde{y}_{m,n,t}^{\pm Q}$ are the sensor m 's corresponding measurements. e_m^T is a row vector that extracts $\tilde{y}_{m,n,t}^{\pm Q}$ from $\tilde{x}_{n,t}^{\pm Q}$. $\tilde{y}_{m,n,t}^{*\pm R}$ considers the maximum normal measurement noise value $\pm 3\sqrt{R_{m,n}}$. $\hat{x}_{m,n,t}^{\pm R}$ are the estimations by $\tilde{y}_{m,n,t}^{*\pm Q}$. $K F_{m,n}$ denotes the intermittent KF algorithm in (3)–(7).

As $\hat{x}_{m,n,t}^{\pm R}$ are the state estimation under maximum positive and negative noise, respectively. We use l_∞ -norm of the vector to determine the normal estimation range as $[TH_{m,n,t}^- = \|\hat{x}_{m,n,t}^{-R}\|_\infty, TH_{m,n,t}^+ = \|\hat{x}_{m,n,t}^{+R}\|_\infty]$ according to (13). Hence, we can determine whether $\hat{x}_{m,n,t}$ by $\tilde{y}_{m,n,t}$ is within $[TH_{m,n,t}^-, TH_{m,n,t}^+]$. If $\hat{x}_{m,n,t}$ is within the range, we set the anomaly sensor flag $I_{m,n,t} = 0$, vice versa.

In large timescale, we utilize $\bar{x}_{n,t}$ as the normal state reference for the anomaly sensor m . That is to extract the sensor m 's corresponding measurement from $\bar{x}_{n,t}$ as $\tilde{y}'_{m,n,t}$ according to e_m^T and add the maximum normal measurement noise to $\tilde{y}'_{m,n,t}$ based on (12). Then we achieve the reference normal measurement range of sensor m as $[\tilde{y}'_{m,n,t}^{-R}, \tilde{y}'_{m,n,t}^{+R}]$. If actual $\hat{y}_{m,n,t}$ measured by the anomaly sensor m remains in $[\tilde{y}'_{m,n,t}^{-R}, \tilde{y}'_{m,n,t}^{+R}]$ for consecutive q times, sensor m recovers from the short-term interference and is classified as a normal sensor after we set $\bar{x}_{n,t}$ as the initial state value of the smart KF.

Remark 2: If no packet is received from the sensor m , i.e., $\varphi_{m,n,t} = 0$, the anomaly detection needs to be delayed until the next successful packet reception.

2) *Multisensor Collaboration for Anomaly Classification at Large Timescale:* Both *sensor interference* and *process disturbance* can cause anomalies in sensor measurements. Sensor interference (or sensor failure) results in difference between sensor measurements and the values of actual states. If we continue to use measurements of the interfered sensor, the controller will generate control commands that do not reflect the actual state of the plants, thus destroying the control performance. Process disturbance directly acts on the physical plants and affects all system states to deviate from the intended state trajectory, so the outputs of most sensors will get “anomaly.” Control performance can also be affected if there is no timely response when a process disturbance occurs. Therefore, we propose collaboration in multiple sensors to distinguish sensor interference and process disturbance at large timescale.

Assuming that the interference among sensors is not correlated, in large timescale, we check $\hat{x}_{m,n,t}, m \in IS_{n,t}$, obtained from their primary KFs to see if they are within the normal state estimation ranges $[TH_{m',n,t}^-, TH_{m',n,t}^+]$ of other sensor ($m', m' \in IS_{n,t} \cup NS_{n,t}$). As a new coordination period T_c begins at time t_1 , if there exists more than one abnormal sensors $m \in IS_{n,t}$ and $m' \neq m$ that \hat{x}_{m,n,t_1} are within the range of

$[TH_{m',n,t_1}^-, TH_{m',n,t_1}^+]$, it is judged that the system has undergone a process disturbance and these sensors are reclassified as normal sensors, i.e., $\forall m \in IS_{n,t}$ and $\forall m' \in IS_{n,t} \cup NS_{n,t}$

$$I_{m,n,t} = \neg \bigvee_{m'=1}^{|IS_{n,t} \cup NS_{n,t}|} \mathbb{1} \left(\|\hat{x}_{m,n,t}\|_\infty \in [TH_{m',n,t}^-, TH_{m',n,t}^+] \right. \\ \left. \wedge \|\hat{x}_{m',n,t}\|_\infty \in [TH_{m,n,t}^-, TH_{m,n,t}^+] \right). \quad (14)$$

If \hat{x}_{m,n,t_1} of all anomaly sensors are still out of the range of $[TH_{m',n,t_1}^-, TH_{m',n,t_1}^+]$ for all m' , or the anomaly sensors' measurements \hat{y}_{m,n,t_1} are still out of the $[\hat{y}_{m,n,t_1}^{-R}, \hat{y}_{m,n,t_1}^{+R}]$ as we illustrate in Section IV-C1, we regard that at time t_1 , all sensors are suffering sensor interference. In the worst case that all sensors are detected to be interfered, it is necessary to detect the fault or replace the sensors manually.

The anomaly sensor detection (ASD) algorithm is outlined in Algorithm 1. This algorithm is divided into two parts. The first part is detecting anomalous sensors, which runs in each T_s . In the second part, the sensor interference and process disturbance are distinguished by collaboration in large timescale. The algorithm finally outputs the normal sensor candidates. Both parts are lightweight with computational complexity less than $O(MN)$.

3) *Smart KF Coordination:* In small timescale, if the main sensor is detected no anomaly, the final estimation result is $\bar{x}_{n,t} = \hat{x}_{\text{main},n,t}$. If $I_{\text{main},n,t} = 1$, the estimation applies the adjoint KF's estimation result based on (9) to achieve a “normal” state estimation based on previous normal states, i.e., $\bar{x}_{n,t} = \hat{x}'_{\text{main},n,t}$, until the beginning of next T_c with an updated main sensor. In large timescale (the first T_s of T_c), if $I_{\text{main},n,t} = 0$, the final estimation result is $\bar{x}_{n,t} = \hat{x}_{\text{main},n,t}$. If $I_{\text{main},n,t} = 1$ in the previous T_c or at the current time, a new main sensor with no anomaly is selected by the SCMS agent from the normal candidate sensors that successfully transmitted the packets at the current time. And the new main sensor's state estimation is applied as the final state estimation $\bar{x}_{n,t} = \hat{x}_{\text{main},n,t}$.

In the extreme case that all sensing packets are lost in the first T_s of T_c , we continue to use the previous main sensor's $\hat{x}_{\text{main},n,t}$ by primary KF as $\bar{x}_{n,t}$. In the case that all sensors are classified as anomalous sensors in the first T_s of T_c , we continue to use the previous main sensor's $\hat{x}'_{\text{main},n,t}$ by adjoint KF as $\bar{x}_{n,t}$ and set $I_{\text{main},n,t} = 0$ until the process disturbance or sensor interference is classified as described in Section IV-C2. If the anomaly is classified as process disturbance, the anomaly detector and coordinator reclassifies the sensors whose measurements are back to normal ranges to normal, and generate estimation result $\bar{x}_{n,t} = \hat{x}_{\text{main},n,t}$ based on the main sensor selection by the SCMS Agent.

Applying $\bar{x}_{n,t} = \hat{x}'_{\text{main},n,t}$ instead of $\hat{x}_{\text{main},n,t}$ when $I_{\text{main},n,t} = 1$ may postpone the response to process disturbances and cause degradation of control performance. However, regarding the sensor interference, we can gain the performance benefit by correct state prediction $\hat{x}'_{\text{main},n,t}$ based on previous normal measurements until a new main sensor is determined. As we can see, let $\bar{x}_{n,t} = \hat{x}'_{\text{main},n,t}$ result in a control performance tradeoff

Algorithm 1: ASD Algorithm

```

input :  $\hat{x}_{m,n,t}, \hat{x}'_{m,n,t}, \bar{x}_{n,t-1}, I_{m,n,t-1}, NS_{n,t}, IS_{n,t}, u_{n,t-1}$ ,
 $Q_n, R_{m,n}, n \in \{1, \dots, N\}, N$  is the total number of
control loops.
output:  $NS_{n,t}$ 
for  $n = 1$  to  $N$  do
    #1 Detect sensor anomaly by the  $3\sigma$  threshold policy.
    for each  $m$  in  $NS_{n,t} \cup IS_{n,t}$  do
        if  $I_{m,n,t-1} \neq 1$  then
            Calculate  $[TH_{m,n,t}^-, TH_{m,n,t}^+]$  for each sensor's state
            estimation by Eqs. (10)–(13).
            if  $\|\hat{x}_{m,n,t}\|_\infty \in [TH_{m,n,t}^-, TH_{m,n,t}^+]$  then
                |  $I_{m,n,t} \leftarrow 0$ .
            else
                |  $I_{m,n,t} \leftarrow 1$ .
            end
        else
            if the anomaly sensor  $m$ 's measurement  $\hat{y}_{m,n,t}$  are
            within the range  $[\hat{y}_{m,n,t}^- - R, \hat{y}_{m,n,t}^+ + R]$  for consecutive  $q$ 
            times then
                |  $I_{m,n,t} \leftarrow 0$ , set the  $\bar{x}_{n,t}$  as initial state.
            else
                |  $I_{m,n,t} \leftarrow I_{m,n,t-1}$ .
            end
        end
    end
    #2 distinguishing process disturbance and sensor
    interference by sensors collaboration.
    if  $t$  is at the beginning of  $T_c$  (the current large timescale)
    then
        for each sensor  $m$  in  $IS_{n,t}$  do
            for  $m' = 1$  to  $M$  do
                if  $m' \neq m$  and
                 $\hat{x}_{m',n,t} \in [TH_{m,n,t}^-, TH_{m,n,t}^+]$  and
                 $\hat{x}_{m,n,t} \in [TH_{m',n,t}^-, TH_{m',n,t}^+]$  then
                    |  $I_{m,n,t} \leftarrow 0, I_{m',n,t} \leftarrow 0$ .
                end
            end
        end
        Update the normal sensor candidates  $NS_{n,t}$ .
    end
return  $NS_{n,t}$ .

```

between process disturbance and sensor interference, which we will evaluate in Section VI.

D. Collaborative KF Updating

Since only the measurements of main sensors $y_{main,n,t}$ are transmitted each T_s except the first one within T_c , the KFs for auxiliary and abnormal sensors have no inputs $\hat{y}_{m,n,t}$ from the industrial plants. As we discussed in Section III-C3, there is a critical bound of the input suspension for KFs, the exceedance of which may result in nonconvergence of the estimation. When auxiliary sensors or recovered sensors become main sensors based on the results of SCMS Agent, the state estimation $\bar{x}_{n,t}$ by new main sensors' primary KFs will be in trouble. Therefore, we propose the KF updating mechanism for auxiliary and abnormal sensors, which operates based on the following strategy.

The collaborative KF updating module collects $IS_{n,t}$ and $NS_{n,t}, \bar{x}_{n,t}$. In small timescale (each T_s except the first one

within T_c), the module extracts stimulated measurements $\bar{y}_{m,n,t}$ using different e_m corresponding to each auxiliary sensor in the normal sensors set $NS_{n,t}$ and transmits to their corresponding smart KFs for updating, respectively. For an anomaly sensor in $IS_{n,t}$ that suffers the sensor interference, its corresponding primary KF updates based on anomaly measurements during the interference, such that diverges from the real state. As a result, the primary KF requires a long time to converge to the real state after the interference ends. To speed up its convergence, when the sensor interference ends, the collaborative KF updating module feeds the $\bar{x}_{n,t}$ as the initial state $\hat{x}_{m,n,t}^-$ for its next iteration process.

E. Dynamic Identification of Physical Plant Parameters

Previously, the SE assumes exact knowledge of the industrial plant. This is not always the case in practice. SE should incorporate adaptation mechanisms to address parametric model uncertainties. In this work, we apply a limit memory recursive least square (LMRLS) algorithm [55] for adaptive estimation of physical parameters. The LMRLS algorithm is applicable for linear or nonlinear systems and supports both offline and online identification. LMRLS uses the fixed-length sliding-window data collection for parameter identification, which is commonly applied for time-varying systems. We define the physical parameter to be identified as $\theta_{n,t}$, and $\hat{\theta}_{n,t}$ is the identification result. First, we reformulate the DT-LTI state-space model of (1) as an auto regressive with exogenous input model (ARX) in

$$A(z^{-1})y_{n,t} = B(z^{-1})u_{n,t} + v_{n,t} \quad (15)$$

where $A(z^{-1}) = 1 + a_1z^{-1} + \dots + a_{n_a}z^{-n_a}$, $B(z^{-1}) = b_1z^{-1} + \dots + b_{n_b}z^{-n_b}$, the coefficient of each term of $A(z^{-1})$ and $B(z^{-1})$ is a function of $\theta_{n,t}$, e.g., $a_1 = f_1(\theta_{n,t})$. n_a, n_b are the orders of $A(z^{-1})$ and $B(z^{-1})$, respectively. The model parameter vector is $\hat{\Theta}_{n,t} = [a_1, \dots, a_{n_a}, b_1, \dots, b_{n_b}]$. The ARX model structure in (15) requires a fixed measurement $y_{n,t}$, i.e., the output matrix C_n is fixed. But our SSCC framework schedules different $y_{m,n,t}$ transmissions based on physics and network status, so the module inputs $\bar{x}_{n,t}$ and extracts the required measurement $\bar{y}_{m,n,t}$ from $\bar{x}_{n,t}$ as $y_{n,t}$ for online identification. Then the formulas of the LMRLS estimation are as follows:

$$K_{n,t} = P_{n,t-1}h_{n,t}^T[I + h_{n,t}P_{n,t-1}h_{n,t}^T]^{-1} \quad (16)$$

$$P_{n,t} = [I + K_{n,t}h_{n,t}]P_{n,t-1} \quad (17)$$

$$\hat{\Theta}_{n,t} = \hat{\Theta}_{n,t-1} - K_{n,t}[\bar{y}_{m,n,t} - h_{n,t}\hat{\Theta}_{n,t-1}] \quad (18)$$

where $K_{n,t}$ is the gain matrix at time t of LMRLS for loop n . $P_{n,t}$ is the covariance matrix at time t . $\hat{\Theta}_{n,t}$ is the estimated parameters $\hat{\Theta}$ at time t . $h_{n,t} = [-\bar{y}_{m,n,t-1}, \dots, -\bar{y}_{m,n,t-n_a}, u_{n,t-1}, \dots, u_{n,t-n_b}]^T$ is the measurement data vector at time t of LMRLS, and $\bar{y}_{m,n,t}$ is the measurement of the plant state at time t .

At each sampling time, LMRLS computes the model parameter vector $\hat{\Theta}_{n,t}$ and derives $\hat{\theta}_{n,t}$ from the elements in $\hat{\Theta}_{n,t}$, e.g., $\hat{\theta}_{n,t} = f_1^{-1}(a_1)$. Finally, the module transmits $\hat{\theta}_{n,t}$ to the smart KFs, controller and SCMS agent to update their knowledge of plant models at run-time.

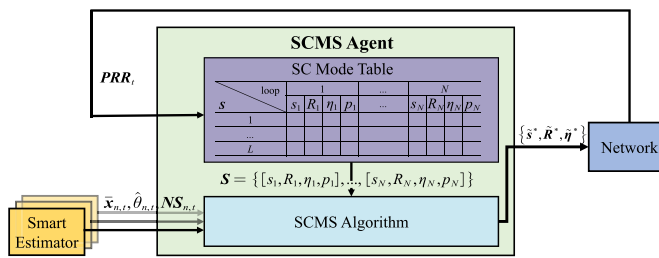


Fig. 7. SCMS agent architecture.

V. SENSING-COMMUNICATION CO-DESIGN

In this section, the SCMS agent is proposed to dynamically select sensors and network configurations, e.g., routing and transmission scheduling, based on sensor selection results, plant states, and the link qualities of the wireless network.

A. Sensing-Communication Mode Switching Overview

Fig. 7 presents the architecture of the SCMS Agent. The SCMS agent operates in each large timescale (the first T_s of T_c). The inputs of SCMS agent are the normal sensor selection result $NS_t = \{NS_{1,t}, \dots, NS_{n,t}, \dots, NS_{N,t}\}$, state estimations $\bar{x}_t = \{\bar{x}_{1,t}, \dots, \bar{x}_{n,t}, \dots, \bar{x}_{N,t}\}$ and identification result $\hat{\theta}_t = \{\hat{\theta}_{1,t}, \dots, \hat{\theta}_{n,t}, \dots, \hat{\theta}_{N,t}\}$ from SEs, and the wireless link quality set PRR_t . The main sensors $s = \{s_1, \dots, s_n, \dots, s_N\}$ and corresponding network configurations, i.e., routing $R = \{R_1, \dots, R_n, \dots, R_N\}$ and transmission scheduling $\eta = \{\eta_1, \dots, \eta_n, \dots, \eta_N\}$ are selected by ideally solving an overall combinatorial optimization problem which is impossible to find the solution in polynomial time [56]. In order to approach the optimal solution, the agent executes the SCMS algorithm by searching a predefined limited-length SC mode table to find a combination of main sensors and corresponding network configurations, which are delivered to the wireless nodes via beacon frames by NM. By designing the SCMS agent and integrating it into NM, the main sensors and network configurations can be dynamically updated according to plant states, sensor status, and network environment changes.

B. Problem Formulation

In this section, we construct a multiobjective optimization problem to minimize the sum of state estimation error, network transmission cost, and switching cost by selecting main sensors and network configurations. To be more specific, the optimization problem has three decision variables $s = \{s_1, \dots, s_n, \dots, s_N\}$, $R = \{R_1, \dots, R_n, \dots, R_N\}$, and $\eta = \{\eta_1, \dots, \eta_n, \dots, \eta_N\}$, where s_n is the main sensor of the loop n , R_n the routing from s_n to one of the access points (APs) under the source routing [57], η_n the number of transmissions allocated to R_n . The objective function $J(s, R, \eta)$ is constructed in (19) and (20) to represent the weighted control and communication costs. The optimal $\{s^*, R^*, \eta^*\}$ can be obtained by minimizing

$$\mathcal{J}(s, R, \eta) = \sum_{n=1}^N J(s_n, R_n, \eta_n) \quad (19)$$

$$J(s_n, R_n, \eta_n) = e^{\alpha V_{n,t}} \tilde{\mathbb{E}}[\|e_{n,t}\|^2 | p(s_n, R_n, \eta_n)] + w_T \text{cost}_T, \{s_n, R_n, \eta_n\} + w_G \text{cost}_G, \{s_n, R_n, \eta_n\}. \quad (20)$$

Notation $p(s_n, R_n, \eta_n)$ is the estimated PDR under s_n , R_n , and η_n . As we denote the total hop count of R_n as hop_{R_n} , and the wireless link of the h th hop within R_n as $R_{n,h}$, the estimated PDR can be expressed as

$$p(s_n, R_n, \eta_n) = \prod_{h=1}^{\text{hop}_{R_n}} (1 - PRR_{R_n,h})^{\eta_n}. \quad (21)$$

$\tilde{\mathbb{E}}[\|e_{n,t}\|^2 | p(s_n, R_n, \eta_n)]$ represents the effect of PDR on the estimation error between the true state $x_{n,t}$ and estimated state $\bar{x}_{n,t}$. According to [37], the expected value of the estimation error with k consecutive packet losses is formulated as (22). Assuming that the end-to-end packet loss probability at any time satisfies the i.i.d. distribution, the probability of k consecutive packet losses with PDR $p(s_n, R_n, \eta_n)$ can be expressed as $(1 - p(s_n, R_n, \eta_n))^k$. By traversing the possibility of consecutive packet losses that range from 0 to ∞ , the effect of $p(s_n, R_n, \eta_n)$ on the estimation error at time t can be expressed as an infinite series in

$$\mathbb{E}[\|e_{n,t}^k\|^2] = \begin{cases} 0, & \text{if } k = 0 \\ \sum_{r=0}^{k-1} \text{Tr}((A_n^T)^r A_n^r Q_n), & \text{if } k > 0. \end{cases} \quad (22)$$

$$\mathbb{E}[\|e_{n,t}\|^2 | p(s_n, R_n, \eta_n)] = \sum_{k=1}^{\infty} \mathbb{E}[\|e_{n,t}^k\|^2] (1 - p(s_n, R_n, \eta_n))^k. \quad (23)$$

Although $\mathbb{E}[\|e_{n,t}^k\|^2]$ increases monotonically as k increases, the convergence of (23) is determined by $\rho(A_n)$. If $\rho(A_n) < 1$, which means the system is stable, (23) converges to a finite value. While $\rho(A_n) \geq 1$, (23) will diverge. In our SSCC, we do not assume that the control loops are all stable or all unstable, and with the continuous improvement of the reliability of the industrial wireless network, a large number of consecutive packet losses is not realistic. Therefore, we only take the first Kr term of (23) to evaluate the effect of PDR on the estimation error of different loops by

$$\tilde{\mathbb{E}}[\|e_{n,t}\|^2 | p(s_n, R_n, \eta_n)] = \sum_{k=1}^{\text{Kr}} \mathbb{E}[\|e_{n,t}^k\|^2] (1 - p(s_n, R_n, \eta_n))^k \quad (24)$$

where $\text{Kr} = \max \text{Kr}_n$, $\text{Kr}_n = \min \text{Kr}_n$, s.t. $(1 - \bar{\lambda}_n)^{\text{Kr}_n} \leq \bar{p}$, as we define that the probability of the upper limit of the consecutive packet drops Kr_n is exactly less than an extremely small value \bar{p} , e.g., $\bar{p} = 10^{-4}$.

$V_{n,t}$ is the value of the Lyapunov function of the n th loop, and we denote $e^{\alpha V_{n,t}}$ as the physical dynamic coefficient, which characterizes the run-time control performance. α is a coefficient that weights the run-time control performance in $J(s_n, R_n, \eta_n)$. A large $e^{\alpha V_{n,t}}$ indicates that the state trajectory is far away from the equilibrium point, which requires a more reliable wireless network. In contrast, a smaller $e^{\alpha V_{n,t}}$ indicates that the state trajectory is closer to the equilibrium point and a deterioration in the quality of the link does not significantly affect control performance. Compared with the

traditional network resource allocation optimization problem with the objective of minimizing a single estimation error, by incorporating $e^{\alpha V_{n,t}}$ in (19) and (20), the estimation error $e_{n,t}$ is dynamically weighted by the run-time plant status.

Notation $\text{cost}_{T,\{s_n, R_n, \eta_n\}}$ is the transmission cost under R_n and η_n , i.e., $\text{cost}_{T,\{s_n, R_n, \eta_n\}} = \text{hop}_{R_n} \eta_n$ and w_T is the transmission cost coefficient. Notation $\text{cost}_{G,\{s_n, R_n, \eta_n\}}$ is the reconfiguration cost of switching to a new $\{s_n, R_n, \eta_n\}$ for control loop n , which is represented by the number of updated transmissions δ with different senders or receivers in each superframe, and w_G is the switching cost coefficient. In Section VI-B1, we perform a thorough evaluation for the selection of the coefficients α , w_T , and w_G .

Substituting (24) into (19), $\mathcal{J}(s, \mathbf{R}, \boldsymbol{\eta})$ is finally represented by

$$\begin{aligned} \mathcal{J}(s, \mathbf{R}, \boldsymbol{\eta}) = & \sum_{n=1}^N \left(e^{\alpha V_{n,t}} \sum_{k=1}^{K_r} \mathbb{E} [\|e_{n,t}^k\|^2] (1 - p(s_n, R_n, \eta_n))^k \right. \\ & \left. + w_T \text{hop}_{R_n} \eta_n + w_G \delta \right). \end{aligned} \quad (25)$$

We finally formulate the SC optimization problem (26)

$$\min_{s, \mathbf{R}, \boldsymbol{\eta}} \mathcal{J}(s, \mathbf{R}, \boldsymbol{\eta}) \quad (26a)$$

$$\text{s.t. } \sum_{n=1}^N \text{hop}_{R_n} \eta_n \leq L_{\text{frame}} \quad (26b)$$

$$p(s_n, R_n, \eta_n) \geq \bar{\lambda}_n \quad (26c)$$

$$s_n \in NS_{n,t}. \quad (26d)$$

The optimization problem provides main sensors and network configurations $\{s, \mathbf{R}, \boldsymbol{\eta}\}$ which can minimize the sum of estimation and communication cost in (25). Equation (26b) indicates the network resource constraints. We denote the superframe length as L_{frame} and the total number of transmissions of N loops should not be larger than L_{frame} . Equation (26c) expresses the minimum requirement of PDR to satisfy the mean state covariance boundedness for all initial conditions, i.e., $p(s_n, R_n, \eta_n) \geq \bar{\lambda}_n$, where $\bar{\lambda}_n$ is illustrated in Section III-C3 as the lower bound PDR for the convergence of $P_{m,n,t}$ in KF. If extremely severe network interference occurs at time t such that any $\{s_n, R_n, \eta_n\}$ for loop n is lower than $\bar{\lambda}_n$, there is no solution of the optimization problem in (26) and the state estimation procedure of KF may lead to an unbounded state error covariance [40]. For such case, we may assign additional retransmissions by scheduling the CAP slots within the superframe to improve the PDR. Equation (26d) ensures the main sensor s_n is detected to be no anomaly by SE.

C. SC Mode Switching Strategy

However, solving the optimization problem (26) is NP-hard [48]. In order to reduce the operational complexity while approximating optimal solution $\{s^*, \mathbf{R}^*, \boldsymbol{\eta}^*\}$ of (26), we define two SC co-design variables: 1) single loop SC mode S_n and 2) overall SC mode S . S_n is a tuple that consists of a main sensor s_n , routing R_n , transmission number η_n , and estimated PDR p_n , i.e., $S_n = [s_n, R_n, \eta_n, p_n]$. An overall SC mode S_i is a combination of S_n for N loops, i.e.,

TABLE II
OVERALL SC MODE TABLE

S	Loop	1				...				N			
		s_1	R_1	η_1	p_1	...	s_N	R_N	η_N	p_N			
	1												
	...												
	L												

$S = \{S_1, \dots, S_n, \dots, S_N\}$. SCMS agent predefines an overall SC mode table that contains L SC modes. Thus, solving the optimization problem is transformed to search within L SC modes and obtain \tilde{S}^* .

The overall SC mode table is shown in Table II, each row in the table contains an overall SC mode S_i . With the experimental setup of multiple control loops with a multihop wireless network in Section VI, an example of SC mode S can be expressed as $S_i = \{S_1, S_2, S_3, S_4\} = \{[S_1, S_1 - R_4 - AP_1, 1, 0.75], [S_4, S_4 - R_3 - AP_2, 1, 0.83], [S_8, S_8 - R_2 - AP_2, 2, 0.92], [S_{12}, S_{12} - R_4 - AP_1, 3, 0.98]\}$ which means that loop 1's main sensor s_1 is S_1 , the routing R_1 from S_1 to AP is $S_1 - R_4 - AP_1$ and $\eta_1 = 1$, the estimated PDR p_1 is 0.75. The sensor and network configurations for the other loops can also be obtained from S_i as loop 1. When constructing the SC mode table, instead of randomly selecting the SC modes, we devise a heuristic approach for selecting SC modes within the predefined SC mode table.

First, initialize the table length L , R_n , η_n , s_n of each loop. Second, the feasible physical state (denoted by $x_{n,t}$) as well as the wireless link quality (denoted by packet reception ratio, PRR) are uniformly divided into multiple intervals. Finally, L optimal SC modes for L network and physical states are obtained by solving the problem (26). Through the above design, the table covers as many physical and network states as possible with a limited length.

In large timescale, the SCMS agent executes the SCMS algorithm (Algorithm 2). The SCMS agent updates estimated PDR p_n based on PRR_t according to (21) for the L SC modes, and searches the SC mode table and determines whether the mode S_i satisfies constraints (26c) and (26d). If so, we predict the performance of (25) for the SC mode S_i . Finally, after searching L SC modes, the SC mode \tilde{S}^* that minimizes (25) is determined, the main sensor set \tilde{s}^* and the network configurations $\tilde{\mathbf{R}}^*$ and $\tilde{\boldsymbol{\eta}}^*$ are sent to the network via NM.

S_i contains N single-loop mode S_n , if we traverse all combinations of single-loop SC modes for N loops to solve (26), the time complexity is $O((M_n)^N)$, where M_n is the total number of $\{s_n, R_n, \eta_n\}$ combinations in loop n . Compared to this brute force search approach, the time complexity is reduced to $O(L)$ by searching L entries from top to bottom in the SC mode table. Although the obtained \tilde{S}^* may be not optimal, we can approach the optimal solution by considering more SC modes in the table. As L approaches $(M_n)^N$, the SCMS result $\{\tilde{s}^*, \tilde{\mathbf{R}}^*, \tilde{\boldsymbol{\eta}}^*\}$ converges to the optimal SC switching result $\{s^*, \mathbf{R}^*, \boldsymbol{\eta}^*\}$. We discuss the difference in performances when the SC mode table is of different lengths L in Section VI-B3.

Algorithm 2: SC Mode Switching (SCMS) Algorithm

input : $PRR_t, NS_t, V_t = \{V_{1,t}, \dots, V_{n,t}, \dots, V_{N,t}\}$,
 $\hat{\theta}_t = \{\hat{\theta}_{1,t}, \dots, \hat{\theta}_{n,t}, \dots, \hat{\theta}_{N,t}\}$, SC mode table
 $S = [S_1, \dots, S_i, \dots, S_L]$.
output: $\tilde{s}^*, \tilde{R}^*, \tilde{\eta}^*$.

$\mathcal{J} \leftarrow 0; \mathcal{J}_{\min} \leftarrow \infty;$
for $i = 1$ to L **do**
 for $n = 1$ to N **do**
 if $p_n > \bar{\lambda}_n$ and $s_n \in NS_{n,t}$ **then**
 $J_n \leftarrow J(s_n, R_n, \eta_n)$,
 $\mathcal{J}_i \leftarrow \mathcal{J}_i + J_n$.
 else
 $\mathcal{J}_i \leftarrow \infty$;
 Break;
 end
 end
 if $\mathcal{J}_i < \mathcal{J}_{\min}$ **then**
 $\mathcal{J}_{\min} \leftarrow \mathcal{J}_i$;
 $\tilde{s}^* \leftarrow [s_1, \dots, s_n, \dots, s_N]$;
 $\tilde{R}^* \leftarrow [R_1, \dots, R_n, \dots, R_N]$;
 $\tilde{\eta}^* \leftarrow [\eta_1, \dots, \eta_n, \dots, \eta_N]$;
 end
end
return $\tilde{s}^*, \tilde{R}^*, \tilde{\eta}^*$.

VI. EVALUATION

This section presents a systematic evaluation of SSCC. The experimental setup is introduced in Section VI-A, and we perform case studies under single and multiple control loops in Section VI-B. Finally, in Section VI-C, SSCC is implemented in real WSAN, and a semi-physical experiment is performed.

A. Experimental Settings

1) *Physical Control System*: Consider four independent 4-state linear load positioning systems [47], which is represented by the DT-LTI state-space model with (1) and (2), where

$$A_n = \begin{bmatrix} 0 & 1 & 0 & 0 \\ 0 & \left(\frac{-d_L}{m_L} + \frac{-d_B}{m_B}\right) & \frac{k_B}{m_B} & \frac{d_B}{m_B} \\ 0 & 0 & 0 & 1 \\ 0 & \frac{d_L}{m_B} & -\frac{k_B}{m_B} & -\frac{d_B}{m_B} \end{bmatrix}, B_n = \begin{bmatrix} 0 \\ \frac{1}{m_L} \\ 0 \\ -\frac{1}{m_B} \end{bmatrix}$$

and C_n updates according to the main sensors selection. Notations d_L, m_L, d_B, m_B , and k_B are the parameters of the load and base platforms. The state vector is $x = [x_L \dot{x}_L x_B \dot{x}_B]^T$, where x_L and \dot{x}_L , x_B and \dot{x}_B are the position and velocity of the load relative to the base platform, the position, and velocity of the base platform, respectively. The balance points of all systems are set to the origin by the linear transformation. The simulation interval is 1200 s, the collaboration period T_c is 1.5 s, and the sampling period T_s is 0.3 s. We apply heterogeneous physical plants, as shown in Table III.

The process noise covariance matrix Q_n of each loop is set to be equal to

$$Q = \begin{bmatrix} 10^{-1} & 0 & 0 & 0 \\ 0 & 10^{-2} & 0 & 0 \\ 0 & 0 & 10^{-1} & 0 \\ 0 & 0 & 0 & 10^{-2} \end{bmatrix}.$$

TABLE III
SYSTEM PARAMETERS INITIALIZATION

Value \ Loop	1	2	3	4
Par				
d_L (N*s/m)	15	15	15	15
m_L (kg)	10	40	150	20
d_B (N*s/m)	0.5	0.2	0.2	0.2
m_B (kg)	50	15	30	10
k_B (N/m)	0.1	0.07	0.07	0.07

TABLE IV
VARIATION OF THE BASE PLATFORM'S DAMPING d_B

Loop	d_B (N*s/m)	Interval (s)	Loop	d_B (N*s/m)	Interval (s)
1	0.5	0~40	2	0.2	0~35
	1	40~150		1.1	35~120
	1.5	150~1200		0.7	120~1200
3	0.2	0~60	4	0.2	0~30
	1	60~300		1.1	30~120
	0.5	300~1200		0.7	120~1200

We deploy three sensors on each load positioning system, which measures x_L, \dot{x}_L , and \dot{x}_B , respectively. Hence, the output matrix C_n of the system can be expressed as follows:

$$C_n = \begin{cases} \begin{bmatrix} 1 & 0 & 0 & 0 \end{bmatrix}, & \text{if sensor measures } x_L \\ \begin{bmatrix} 0 & 0 & 1 & 0 \end{bmatrix}, & \text{if sensor measures } x_B \\ \begin{bmatrix} 0 & 0 & 0 & 1 \end{bmatrix}, & \text{if sensor measures } \dot{x}_B \end{cases}$$

The measurement noise covariance of each output is set to be $R_{x_L} = 10^{-1}, R_{x_B} = 10^{-1}, R_{\dot{x}_B} = 10^{-2}$.

We apply model predictive controllers (MPCs) [58]. The objective function of the quadratic programming problem in MPC can be proved to be a Lyapunov function, which we use as $V_{n,t}$ in (26). Knowing the exact models of the physical plants is only sometimes the case in practice. The parameters of the load positioning systems may change over time. In our case study, parameter mismatches are represented by d_B changes in Table IV. We incorporate the LMRLS described in Section IV-E at each T_s to address parametric model uncertainties.

As shown in Table V, we simulate sensor interference by adding Gaussian noise with nonzero-mean or fixed bias to the measurements. We use $\mathcal{N}(\mu, \sigma)$ to denote the distribution of the Gaussian noise. In particular, when $\sigma = 0$, it is equivalent to adding a fixed bias to the measurement. NT stands for the normal test, and ST stands for the stress test that faces harsh operation environment. In order to evaluate the capability of differentiating process disturbance and sensor interference, we add impulse process disturbance to \dot{x}_B , the disturbance time for loops 1 and 2 is set to $t_{pd} = 600$ s, for loops 3 and 4, $t_{pd} = 300$ s.

To evaluate the control performance, we use the mean absolute error (MAE) in (27), where K is the number of samples and x_{ref} is the reference state

$$\text{MAE} = \frac{1}{K+1} \sum_{k=0}^K |x(k) - x_{\text{ref}}(k)|. \quad (27)$$

TABLE V
SENSOR INTERFERENCE. (a) SINGLE LOOP SIMULATION.
(b) MULTIPLE LOOPS SIMULATION

Loop	Sensor	Noise		Interval (s)
		NT	ST	
2	S4	$\mathcal{N}(2, 1)$	$\mathcal{N}(4, 1)$	165~300 651~750
	S5	$\mathcal{N}(2, 1)$	$\mathcal{N}(4, 1)$	30~100 690~780
	S6	$\mathcal{N}(0.6, 0)$	$\mathcal{N}(1, 0)$	60~120 450~540

Loop	Sensor	Noise		Interval (s)
		NT	ST	
1	S1	$\mathcal{N}(1, 0.5)$	$\mathcal{N}(2, 0.5)$	540~600
	S2	$\mathcal{N}(2, 2.4)$	$\mathcal{N}(8, 2.4)$	150~300
	S3	$\mathcal{N}(1, 0)$	$\mathcal{N}(2, 0)$	240~270
2	S4	$\mathcal{N}(1, 2)$	$\mathcal{N}(3, 2)$	150~270
	S5	$\mathcal{N}(1, 0)$	$\mathcal{N}(2, 0)$	108~200
	S6	$\mathcal{N}(1, 0)$	$\mathcal{N}(2, 0)$	360~510
3	S7	$\mathcal{N}(1, 0.3)$	$\mathcal{N}(2, 1)$	240~270
	S8	$\mathcal{N}(2, 0)$	$\mathcal{N}(7, 0)$	360~450
	S9	$\mathcal{N}(1, 0.5)$	$\mathcal{N}(2, 0.5)$	480~510
4	S10	$\mathcal{N}(1, 1)$	$\mathcal{N}(5, 1)$	240~270
	S11	$\mathcal{N}(1, 0)$	$\mathcal{N}(2, 0)$	240~330
	S12	$\mathcal{N}(1, 0.3)$	$\mathcal{N}(2, 0.3)$	480~510

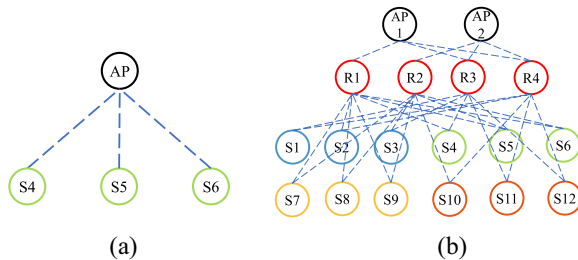


Fig. 8. Wireless network topology. (a) Single-hop network. (b) Multihops network.

2) *Wireless Network*: We simulate an IEEE 802.15.4 beacon-enabled wireless network within TOSSIM. Each superframe has 18 time slots within the CFP, and the time slots are set to 10 ms. The node IDs are shown in Fig. 8(b), S1~3, S4~6, S7~9, and S10~12 belong to Loop 1, 2, 3, and 4, respectively. The three sensors in each loop measure x_L , x_B , and \dot{x}_B . R1~4 are the relay nodes of the multihop network. AP1 and AP2 are the APs of the network. The received signal strength indicator (RSSI) of each wireless link is constantly -67 dBm, and we simulate network interference by changing background noise. We apply two different noise strengths in NT and ST, as shown in Table VI. We set the background noise strength as -80 dBm except for interfered intervals in the table.

B. Sensing-Communication Co-Design

1) *Selection of Coefficients*: In (25), there exist three coefficients w_T , w_G , and α that effect the SC mode

TABLE VI
NETWORK INTERFERENCE. (a) SINGLE LOOP SIMULATION.
(b) MULTIPLE LOOPS SIMULATION

Link	Noise(dBm)		Interval (s)
	NT	ST	
S4-AP	-78	-74	20~90 615~720
S5-AP	-78	-74	100~200 780~840
S6-AP	-78	-74	268~360 450~540

Link	Noise (dBm)	Interval (s)	Link	Noise (dBm)	Interval (s)
R2-AP2	-75	20~85	R4-AP2	-75	20~85
R1-AP1	-75	20~210	R3-AP2	-75	20~210
S7-R2	-78	55~210	S11-R4	-78	55~210
S6-R2	-78	108~285	S5-R1	-78	108~285
S3-R2	-78	135~210	S2-R1	-78	135~210
S9-R2	-75	135~390	S12-R4	-75	900~1000

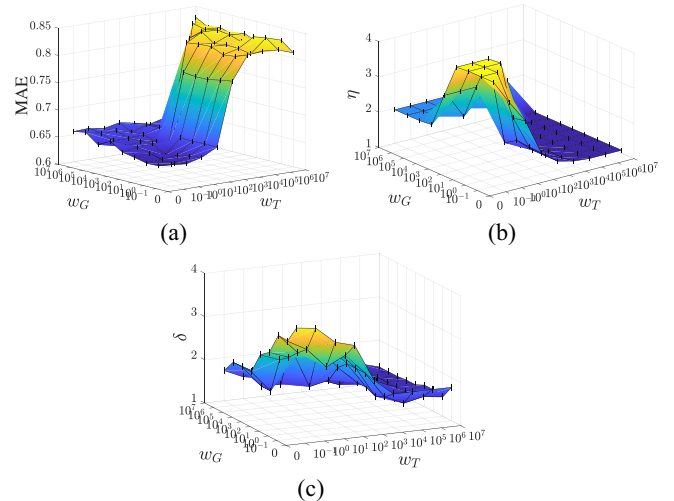


Fig. 9. Performances under different w_T and w_G . (a) MAE. (b) Average η . (c) Average δ .

selection result. We evaluate the control performance, average transmission number η , and average updated time slots number δ under different w_T , w_G , and α .

In Fig. 9, when w_T and w_G are small, SCMS agent selects the SC mode with high-network reliability with the goal of control performance improvement. e.g., when $w_T = w_G = 1$, average η is approximately equal to the maximum transmission number $\eta = 4$ and the control performance is improved by reliable network configuration with $MAE \approx 0.63$. When w_T and w_G are larger, SCMS agent tends to select a SC mode with the goal of saving network resources and reducing switching. e.g., when $w_T = w_G = 10^7$, $MAE \approx 0.85$, average $\eta \approx 1.4$. We can see that when $w_T \leq 10$ and $w_G \leq 10^2$, the control performance does not vary much, but there is a significant decrease in η and δ . This is because SSCC dynamically allocates network resources based on the physical state, which ensures control performance while saving overall network resources and reducing switching. To balance

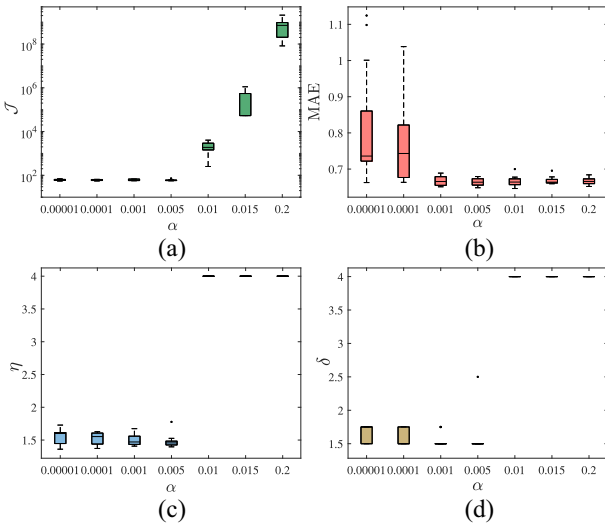


Fig. 10. Performances under different α ($w_T = w_G = 10$). (a) Average \mathcal{J} . (b) MAE. (c) Average η . (d) Average δ .

the improvement of control performance with the reduction of network energy consumption and switching, we set $w_T = 10$ and $w_G = 10$ for single-loop case studies, $w_T = 20$ and $w_G = 10$ for multiloop case studies. When $w_T = w_G = 10$, we test the effect of α . As shown in Fig. 10, when $\alpha \leq 10^{-4}$, due to the small weight of control performance in the cost function, SCMS agent switches to the SC mode that tends to save more network costs. When $\alpha \geq 0.01$, with the increase of the weight of the control performance, high-network reliability is achieved throughout the whole operation interval at the cost of network resources. Therefore, we choose $\alpha = 0.005$ for both single-loop and multiloop case studies to balance the improvement of control performance with the network costs.

2) *Single Control Loop*: Fig. 11 shows the SSCC mechanism for a single loop. At $t = 30$ s, the SE detects a sensor anomaly in S5, and the SCMS agent switches the main sensor to S6 at $t = 30.3$ s, and the η is set to 3 due to the physical state. At $t = 60$ s, S6 is detected anomalous, and the SCMS agent switches to S4 at $t = 60.6$ s. From 160 to 195 s, the SCMS agent reduces η from 3 to 1 as the system state trajectory approaches the equilibrium point. At $t = 268$ s, the route S6-AP's noise strength changes from -80 to -74 dBm. The SCMS agent switches the route from S6-AP to S5-AP instead of increasing η on S6-AP at $t = 270.3$ s. At $t = 601.8$ s, the control performance deteriorates due to the process disturbance that makes the system deviate from the equilibrium point, so the SCMS agent sets $\eta = 2$. At $t = 615$ s, the route S4-AP's noise strength changes from -80 to -74 dBm, the SCMS agent sets $\eta = 3$ on S4-AP for reliable network at $t = 619.8$ s. η is set from 2 to 1 at $t = 751.8$ s as the physical plant converges to the steady state once again. From Fig. 11(f), it can be seen that SSCC can ensure high-network reliability during the transition period, thus ensuring high reliability of state estimation as shown in Fig. 11(g). Therefore, the whole system dynamically adjusts the network configuration based on the physical and network states to realize the co-design of sensing and communication.

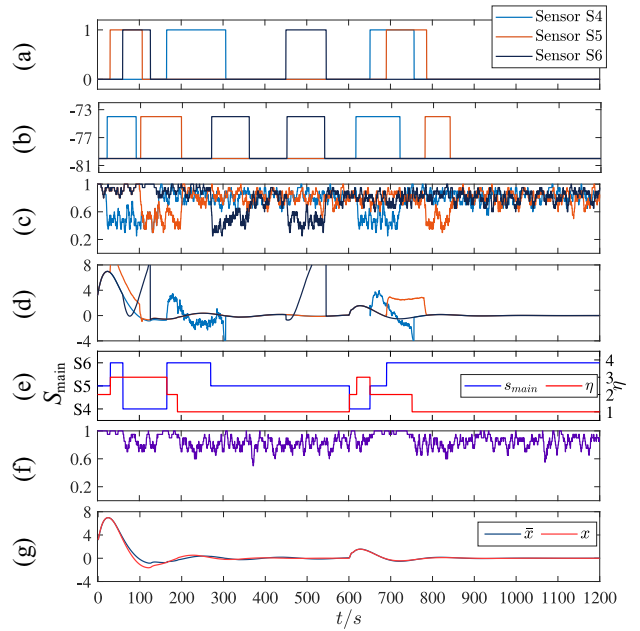


Fig. 11. SSCC results on a single control loop. (a) Sensor interference. (b) Noise/dBm. (c) PRR. (d) \hat{x}_B/m . (e) SC mode. (f) PDR (g) \hat{x} and x_B/m .

We apply the state-of-art robust extended KF (IS-EKF) in [17] as a benchmark to compare with SSCC. In [17], the IS-EKF can handle the measurement outliers of different magnitudes, types, and durations, which corresponds to the irregular noise on the measurements due to sensor interference in realistic scenarios. Since IS-EKF does not consider the packet loss in wireless networks, we enhance the update procedure of the IS-EKF by the intermittent KF [40], which deals with packet losses. The innovation saturation mechanism in [17, eqs. (10a) and (10b)] requires the selection of four parameters λ_1 , λ_2 , γ_1 , and γ_2 . According to the selection suggestions in [17, Remark 4], we set $\lambda_1 = \lambda_2 = 0.75$, $\gamma_1 = \gamma_2 = 1$. Other experimental settings are the same as those in Sections VI-A1 and VI-A2. We perform the comparison with IS-EKF and the other four groups of simulations.

- 1) Our SSCC method, configuring sensors and configuring network (CSCN), where SCMS agent dynamically configures sensors S4~6 and η from 1 to 4.
- 2) IS-EKF with the fixed sensor S5 and fixed network configurations with $\eta = 2$.
- 3) Configuring sensors but fixed network configurations with $\eta = 2$ (CSFN).
- 4) Fixed sensors to S5 but configuring network (FSCN).
- 5) Fixed sensors to S5 and fixed network configurations with $\eta = 2$ (FSFN).

We statistics the control performance under NT and ST cases for both sensor and network interferences in Tables V and VI. As shown in Figs. 11 and 14, it can be seen that the CSCN can ensure stable control performance in the cases of both NT and ST. For IS-EKF, the innovation saturation mechanism dynamically limits the range of outliers. However, since the saturation boundary is not always the real value of the innovation without anomaly when interference happens, the estimation result $\hat{x}_{m,n,t}$ would also be affected by the sensor interference, as shown in Fig. 12(a). The control

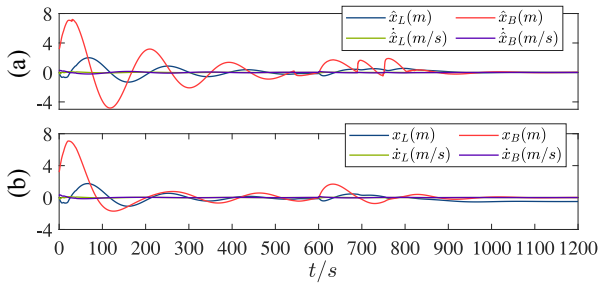


Fig. 12. Results of IS-EKF on a single control loop (ST case). (a) State estimation \hat{x} . (b) Response curve x .

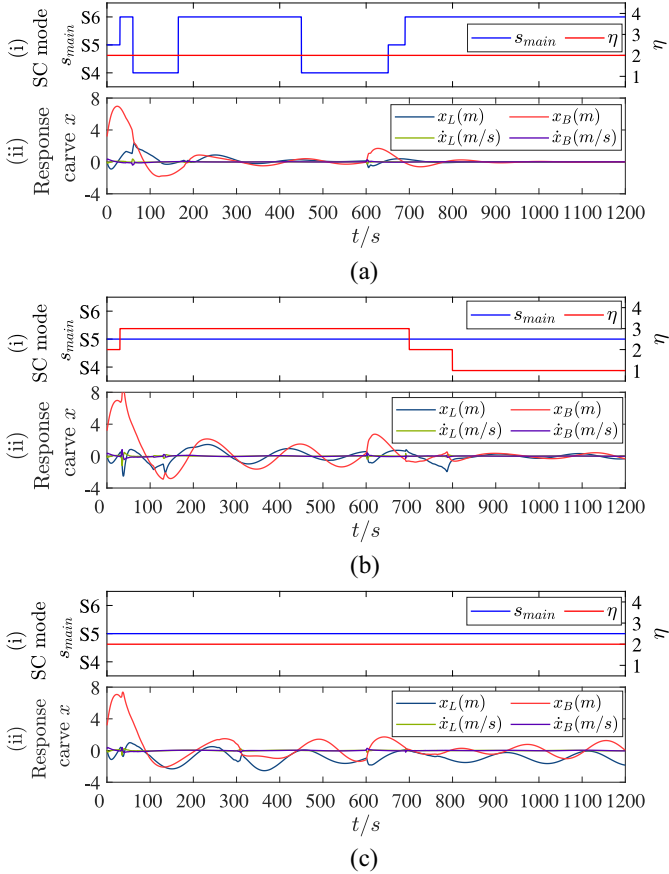


Fig. 13. Results of other SC strategies (ST case). (a) CSFN results. (b) FSCN results. (c) FSFN results.

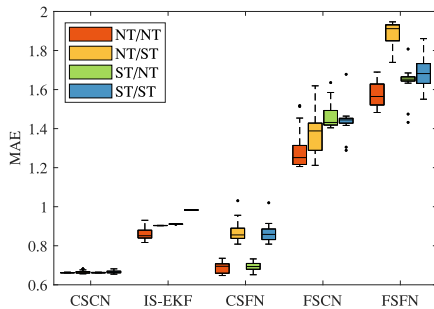


Fig. 14. Control performance of IS-EKF and different SC strategies.

performance of IS-EKF recorded in Fig. 14 under different cases is all within the range of [0.8 1], whose performance is better than the FSCN and FSFN strategies. For CSFN, the noise strength from S4 to the AP increases at $t = 20$ s from

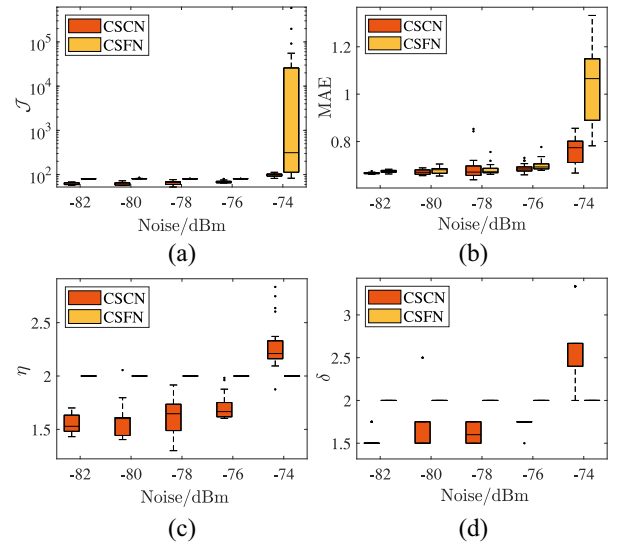


Fig. 15. Performances under different background noises. (a) Average \mathcal{J} . (b) MAE. (c) Average η . (d) Average δ .

-80 to -74 dBm, and a fixed transmission number ($\eta = 2$) cannot always achieve reliable state estimation, thus making the control performance worse due to the parameter identification under a large number of packet loss. FSCN configures the network due to network interference but always regards $\hat{y}_{m,n,t}$ obtained from S5's primary KF as $\bar{x}_{n,t}$ when S5 is interfered, the control performance is worse than CSFN, as shown in Figs. 13(b) and 14. The control performance gets worst compared with other SC strategies as shown in Figs. 13(c) and 14. CSFN's control performance is relatively better compared with FSCN and FSFN due to the timely response to sensor anomaly. Both FSCN and FSFN feed $\hat{y}_{m,n,t}$ obtained from S5's primary KF as $\bar{x}_{n,t}$ to the controller, the control performance deteriorates sharply under both the NT and ST cases, revealing the profound impact of sensor interference on the IIoT-based control system and the necessity of the constraint (26d).

We perform experiments of CSCN and CSFN under different background noise levels, as shown in Fig. 15. SSCC has better control performance under the noises from -82 to -76 dBm in Fig. 15(b). From Fig. 15(c), we can see that SSCC adaptively increases η to achieve high-network reliability, so control performance can be maintained as the noise strength increases.

After evaluating the performance of SSCC with a single loop, we present and analyze the details inside the SE. SE detects the sensor anomalies and estimates the states. If the main sensor is detected to be anomaly in small timescale (each T_s except the first one within T_c), then we set $\bar{x}_{n,t} = \hat{x}'_{m,n,t}$ until the next T_c begins. Process disturbance can also cause anomalies in measurements $y_{m,n,t}$ by moving states away from the original trajectory. Feeding $\hat{x}'_{m,n,t}$ directly to the controller may degrade control performance due to untimely responses to process disturbance. We evaluate the drawback and benefit of regarding $\hat{x}'_{m,n,t}$ obtained from the adjoint KF as $\bar{x}_{n,t}$ when anomalies occur.

The sensor and network interferences are both under NT case. We denote the case of letting $\hat{x}'_{m,n,t}$ be $\bar{x}_{n,t}$ as M_1 , and letting $\hat{x}_{m,n,t}$ be $\bar{x}_{n,t}$ as M_2 . As shown in Fig. 16, at

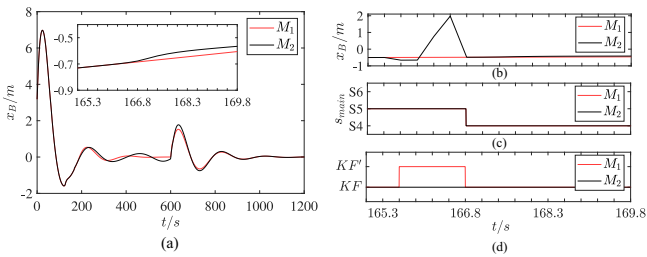


Fig. 16. Results of letting $\hat{x}'_{m,n,t}$ (M_1) and $\hat{x}_{m,n,t}$ (M_2) be $\bar{x}_{n,t}$, respectively, under sensor interference. (a) Response curve x . (b) Zoom in of \bar{x} for [165, 169.8] s. (c) Zoom in of s_{main} for [165, 169.8] s. (d) Zoom in of KF and KF' selection for [165, 169.8] s.

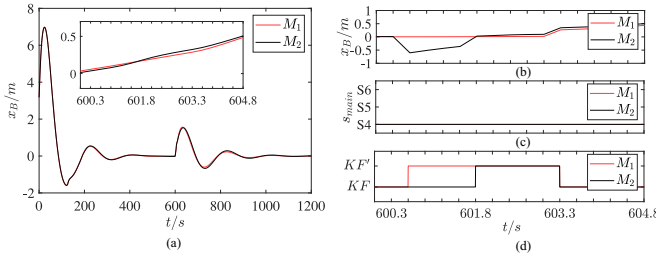


Fig. 17. Results of letting $\hat{x}'_{m,n,t}$ (M_1) and $\hat{x}_{m,n,t}$ (M_2) be $\bar{x}_{n,t}$, respectively, under process interference. (a) Response curve x . (b) Zoom in of \bar{x} for [600, 604.8] s. (c) Zoom in of s_{main} for [600, 604.8] s. (d) Zoom in of KF and KF' selection for [600, 604.8] s.

$t = 165.6$ s, SE receives $\hat{y}_{m,n,t}$ from S5 and detects the anomaly. In Fig. 16(b), M_2 continuously uses the anomaly measurement $\hat{y}_{m,n,t}$ obtained from S5 for state estimation, causing a significant abrupt change in $\bar{x}_{n,t}$. At $t = 166.8$ s, the SCMS agent switches the main sensor s_2 to S4 and $\bar{x}_{n,t}$ is set to be $\hat{x}_{m,n,t}$ which is from S4's primary KF. From the response curve in Fig. 16(a), it can be seen that the control performance degrades after using $\hat{x}_{m,n,t}$ obtained from S5's primary KF as the input to the controller during [165.6 166.5] s. In Fig. 17, we show the difference in control performance while x_B is disturbed under M_1 and M_2 , respectively. At $t = 600.6$ s, SE detects anomaly in $\hat{x}_{m,n,t}$ from S4's primary KF, then M_1 using $\hat{x}'_{m,n,t}$ obtained from S4's primary KF as $\bar{x}_{n,t}$ and M_2 using $\hat{x}_{m,n,t}$ obtained from S4's adjoint KF. At $t = 601.8$ s, SE detects that all sensors of loop 2 are anomaly within [600.6 601.8] s and after 601.8 s both M_1 and M_2 use the $\hat{x}'_{m,n,t}$ obtained from S4's adjoint KF as $\bar{x}_{n,t}$. The primary KF's state estimation $\hat{x}_{m,n,t}$ of all sensors at $t = 603.3$ s satisfy the normal intervals as illustrated in Section IV-C1, and S4, S5, and S6 are reclassified as normal sensors in loop 2's $NS_{n,t}$.

The results show that after the anomalies are detected within T_c , using $\hat{x}'_{m,n,t}$ as $\bar{x}_{n,t}$ until the next T_c beginning improves control performance under sensor interference, which can illustrate the advantage of applying both primary and adjoint KFs in smart KF. When process disturbances occur, this state estimation strategy delays the response to physical state changes. But from the comparison with M_2 , the control performance is not greatly affected. In order to reduce the control performance degradation due to sensor interference, we finally use $\hat{x}'_{m,n,t}$ as $\bar{x}_{n,t}$ until the next large timescale. In addition, we can detect and distinguish anomalies more timely

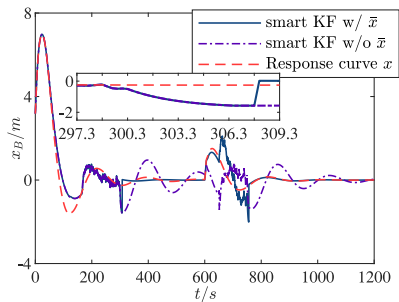


Fig. 18. Results of smart KF with (w/) $\bar{x}_{n,t}$ and without (w/o) $\bar{x}_{n,t}$ after the sensor recovery.

by decreasing T_s or T_c . However, we need to consider the tradeoff between control performance and network costs.

Fig. 18 shows the simulation result that uses S4 and $KF_{4,2}$ as an example to compare the state estimation of smart KF with/without $\bar{x}_{n,t}$ as the initial value after the sensor recovers from the interference. The zoom-in figure in Fig. 18 shows that after the recovery of S4 at $t = 300$ s, anomaly detector and coordinator sdetects that $\hat{y}_{m,n,t}$ from S4 is within the interval $[\hat{y}_{m,n,t}^{(-R)}, \hat{y}_{m,n,t}^{(+R)}]$ of S4 for 6 consecutive T_c from 300.3 s to 309.3 s. Collaborative KF Updating module inputs $\bar{x}_{n,t}$ to $KF_{4,2}$ as the initial value for further prediction and updating. As we can see, the result shows that using $\bar{x}_{n,t}$ as the initial state after sensor interference reduces the filtering convergence time.

3) *Multiple Control Loops*: We perform simulations using four control loops and a multihop IEEE 802.15.4 wireless network. We first select a suitable mode table length L , and then we show the results of the SCMS algorithm. The simulation results verify that our SSCC is equally effective in improving the overall control performance while reducing the network costs in a balanced manner when multiple loops coexist. Finally, we discuss the relationship between switching cost and SC mode table length.

Fig. 19 shows the statistics of the cost function value \mathcal{J} , overall MAE, η , and the execution time of SCMS algorithm for different SC mode table length L . The algorithm execution time is calculated on a 1.8 GHz Intel Core i7 processor. When $L < 5$, the number of SC modes is too small that makes the system continues to use SC modes with sensor interference, making the performance of the multiloop control system deteriorate, which in turn makes the value of the objective function large, as shown in Fig. 19(a). When $L \geq 5$, the system can switch effectively in case of sensor interference. When $L = 1000$, the control performance converges to a constant control performance. As can be seen from Fig. 19(c), η is not monotonically decreasing with L . When $L < 10$, average η depends on the number of transmissions for a few SC modes. As $L \geq 10$, the average η gradually decreases and finally converges to 1.47. Fig. 19(d) shows the statistics of the average execution time of the SCMS algorithm. The execution time keeps increasing as L increases. The execution time can be maintained within 10 ms when $L \leq 1000$. Therefore, we choose $L = 100$ as the length of SC mode table for our multiloop simulation.

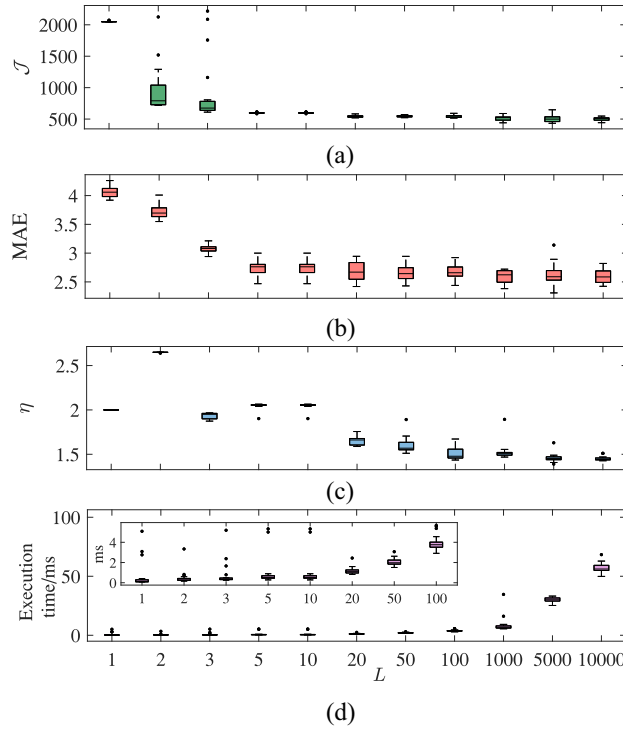


Fig. 19. Performances under different mode table length L . (a) Average \mathcal{J} . (b) MAE. (c) Average η . (d) Average execution time.

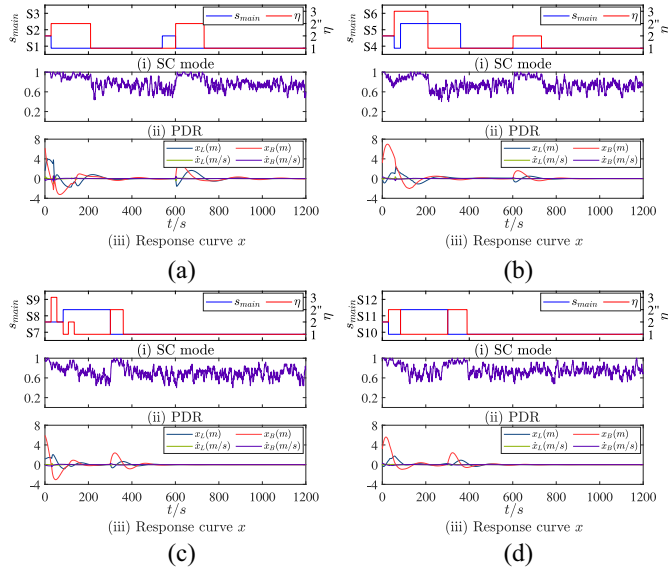


Fig. 20. SSCC (CSCN) results of multiple control loops. (a) Loop 1. (b) Loop 2. (c) Loop 3. (d) Loop 4.

Fig. 20 shows the selection of the main sensors s_{main} and η for the four loops, PDR, and the response curves. The sensor interference settings and network noise are shown in Tables V and VI. For routing switching, we set up two routes with the same η but using different wireless links for each loop denoted as $\eta = 2$ and $\eta = 2''$.

The SCMS agent switches SC mode of the overall multiloop control system based on the physical states, sensor status, or network status. From each subfigure of Fig. 20, it can be found that SSCC can ensure high-wireless network reliability during

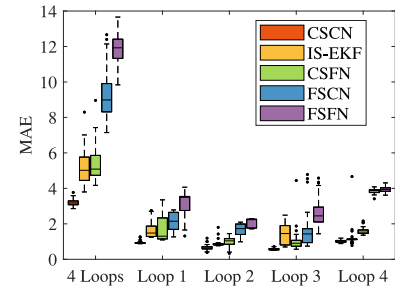


Fig. 21. Control performance under different SC strategies.

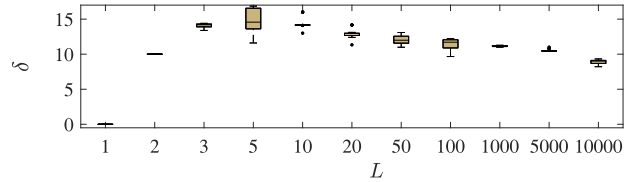


Fig. 22. Average δ under different table length L ($w_G=1000$).

the transition period of the plants while reducing η when the control system converges to the equilibrium point, thus saving network resources.

We also compare with the IS-EKF and evaluate the effect of whether or not to configure sensors and network on the control performance of the multiple loops, where both sensor interference and network background noise settings are under the ST case. Although the total MAE of IS-EKF is approximately equal to that of CSFN in the multiloop case, we find its selection of the parameters in IS-EKF is critical but nontrivial. The state estimation has a higher probability of divergence if the parameters are not properly selected. It is also evident from Fig. 21 that the impact of sensor interference on the overall control system is greater than the impact of network interference on control performance. The control performance by CSCN is improved by three times compared to FSFN.

Since the reconfiguration of wireless networks is sometimes expensive and there is a possibility of reconfiguration failure, we set $w_G = 1000$ to increase the weight of network reconfiguration and compare the reconfiguration costs under different L . As shown in Fig. 22, when $L \leq 5$, the control performances are worse due to the limited SC modes. Therefore, the control performance is improved as much as possible at the cost of more network reconfigurations. When $L > 5$, as the number of candidate SC modes increases, the SC modes obtained by the SCMS algorithm can reduce the network reconfigurations (δ) gradually, which means that each network reconfiguration utilizes the previous network schedule as much as possible, thus reducing the cost of network reconfiguration. We can balance the network reconfiguration costs and the control performance improvement by setting w_G rationally.

C. Semi-Physical Simulation

1) *System Design and Implementation:* We implement and evaluate SSCC in semi-physical simulation. The simulation comprises two computation platforms and a star-WSAN with four TelosB nodes, as shown in Fig. 23. The physical plant and actuator are simulated in MATLAB/Simulink desktop

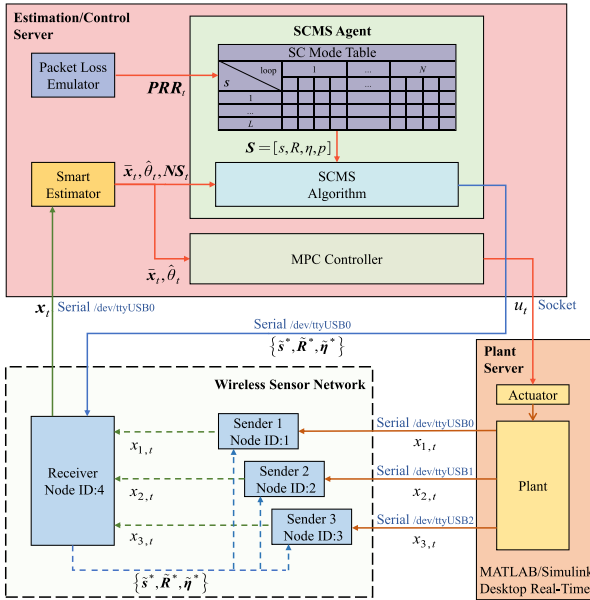


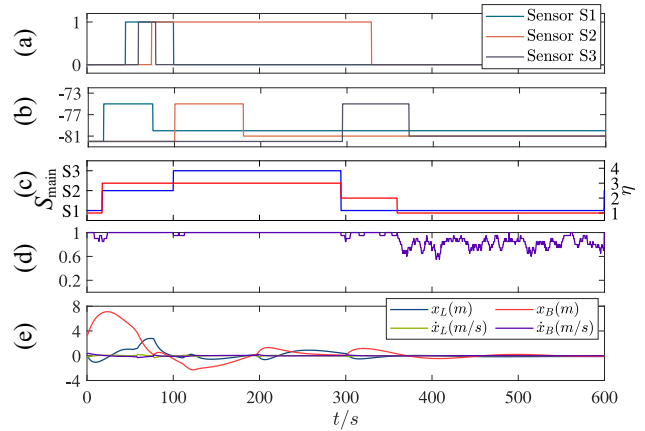
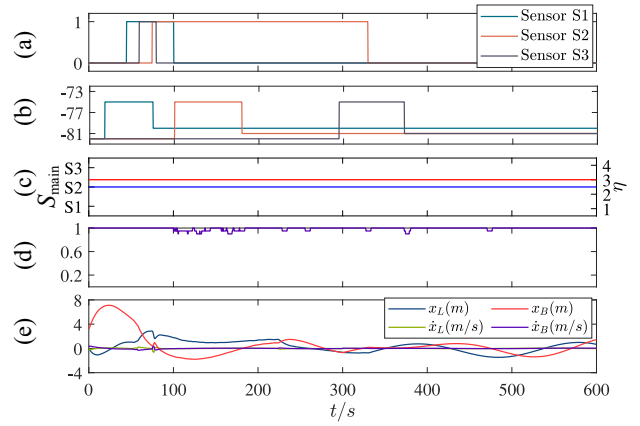
Fig. 23. Semi-physical experiment architecture.

real-time (SLDRT), running on the computation platform called the Plant Server. The second computation platform is the Estimation/Control Server, where the SCMS agent and the MPC controller are implemented. The Plant Server and Estimation/Control Server provide I/O interfaces for connecting TelosB nodes. Three TelosB nodes connecting to the Plant Server serve as the sensors, and one as the coordinator connecting to SE directly. The TelosB nodes communicate with each other over the wireless network based on the IEEE 802.15.4 MAC and the transmission schedule.

As the uplink of our system, the Plant in SLDRT sends sensor data $\{x_{1,t}, x_{2,t}, x_{3,t}\}$ to corresponding TelosB nodes through USB. The three TelosB nodes then transmit each sensor data to the fourth node, which forwards the data to the Estimation/Control Server. And along the downlink, Estimation/Control server calculates: 1) control commands u_t and 2) updated sensing and communication schedule $\{\tilde{s}^*, \tilde{R}^*, \tilde{\eta}^*\}$. Then u_t is fed to the actuator in SLDRT by socket, and the updated transmission schedule $\{\tilde{s}^*, \tilde{R}^*, \tilde{\eta}^*\}$ is sent back to the forth node for wireless network update next superframe.

We implement our SSCC framework over IEEE 802.15.4 time division multiple access (TDMA) network in Contiki OS. The coordinator packages and broadcasts beacon frames with updated transmission schedule $\{\tilde{s}^*, \tilde{R}^*, \tilde{\eta}^*\}$. Other nodes receive the beacon frame and update their schedule based on its next superframe. The experiment setup of the plant is introduced in Section VI-A. For the semi-physical experiment, the control period is set to 0.3 s, and the duration of each round of the experiment is 600 s. And to emulate a network condition with packet losses in a controlled fashion, we utilize TOSSIM traces to intentionally drop packets on the Estimation/Control Server [59], [60].

2) *Experimental Results:* The semi-physical experiments are conducted in two cases: 1) CSCN and 2) FSFN. We set up the semi-physical system with sensor and network interference as shown in Figs. 24 and 25(a) and (b). The advantages of

Fig. 24. SSCC (CSCN) results. (a) Sensor interference. (b) Noise/dBm. (c) SC mode. (d) PDR (e) Response curve x .Fig. 25. FSFN results. (a) Sensor interference. (b) Noise/dBm. (c) SC mode. (d) PDR (e) Response curve x .

our SSCC against both network and sensor interference are indicated by the following.

1) Our SSCC will correctly detect wireless and sensor interferences and successfully switch SC mode, including the sensor selections and the corresponding transmission number. As shown in Fig. 24(a) and (d), at $t = 100$ s, the wireless noise on sensor S2 gets large, so the main sensor is switched to S3. At $t = 295$ s, the noise increases on sensor S3, so the mode switches. Since sensor S2 currently undergoes interference, SSCC chooses sensor S1 instead of sensor S2. At $t = 75$ s, even though the sensor interference is set, the mode is not switched because the criteria for switching are not met at this time. SSCC chooses $\eta = 3$ and gradually decreases η as the state converges.

2) Comparing Figs. 24 and 25, we can see that SSCC could improve the control performance. In FSFN, the main sensor is always selected as S2, and η is set to 3, making the PDR be maintained at a high level. Despite that, the sensor interference destroys the control performance. While in CSCN, our SSCC could switch mode based on wireless noise and sensor interference at run-time, maintaining control performance even undergoing both network and sensor interferences.

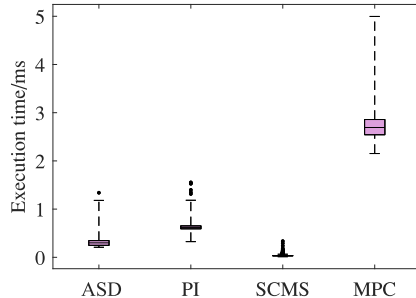


Fig. 26. Execution time statistics for each part on estimation/control server.

Additionally, we have recorded the overhead for each component on the Estimation/Control Server 5000 times, including the ASD algorithm, PI, SCMS algorithm, and MPC Controller. As shown in Fig. 26, the mean overhead summation of the SSCC algorithm (ASD and SCMS) is only 9.7% of the average execution time of PI and MPC, which can demonstrate that our SSCC is lightweight. SSCC can also satisfy the control constraints, as the total worst computing time of the MPC and SSCC is 8.3 ms, which is far less than the superframe duration of 300 ms in our case study.

VII. CONCLUSION

In this article, we have proposed an SSCC framework to enhance the performance of IIoT-based control systems under sensor and network interferences. The SSCC consists of a SE and an SCMS Agent. The SE performs normal sensor selection and resilient state estimation. The SCMS agent searches a predefined SC mode table to select the sensing and communication modes based on a combination of physical plant states, sensors and network status. We have implemented the SSCC both in the WCPS simulator and a real WSAN composed of TelosB nodes. A case study that systematically explores both control and network performances under single-hop and multihop wireless networks has been presented using real-world wireless traces. Both simulation and semi-physical experiment results show that our SSCC can dynamically select sensors and network configurations based on physical states, sensor and network status. These results shed light on a new family of state estimation under wireless network and SC co-design that provides reliable state estimation while saving network resources.

REFERENCES

- [1] C. Lu et al., “Real-time wireless sensor-actuator networks for industrial cyber-physical systems,” *Proc. IEEE*, vol. 104, no. 5, pp. 1013–1024, May 2016.
- [2] W. Rong, G. T. Vanan, and M. Phillips, “The Internet of Things (IoT) and transformation of the smart factory,” in *Proc. Int. Electron. Symp. (IES)*, 2016, pp. 399–402.
- [3] P. Park, S. C. Ergen, C. Fischione, C. Lu, and K. H. Johansson, “Wireless network design for control systems: A survey,” *IEEE Commun. Surveys Tuts.*, vol. 20, no. 2, pp. 978–1013, 2nd Quart., 2018.
- [4] A. Ahlén et al., “Toward wireless control in industrial process automation: A case study at a paper mill,” *IEEE Control Syst. Mag.*, vol. 39, no. 5, pp. 36–57, Oct. 2019.
- [5] B. Ramos et al., “A performance comparison of WirelessHART and ZigBee in oil refinery,” in *Proc. IEEE/APS Topical Conf. Antennas Propag. Wireless Commun. (APWC)*, 2018, pp. 846–849.
- [6] H. Cui and L. Denghua, “Research on electromagnetic interference resistance of piezoelectric vibration acceleration sensor,” *Ferroelectrics*, vol. 460, no. 1, pp. 82–97, 2014.
- [7] A. Aurora, “Algorithmic correction of MOS gas sensor for ambient temperature and relative humidity fluctuations,” *IEEE Sensors J.*, vol. 22, no. 15, pp. 15054–15061, Aug. 2022.
- [8] Y. Wang, J. Xiong, and D. W. C. Ho, “Distributed LMMSE estimation for large-scale systems based on local information,” *IEEE Trans. Cybern.*, vol. 52, no. 8, pp. 8528–8536, Aug. 2022.
- [9] Y. Feng, X. Chen, and Y. Tan, “An improved paradigm for robust optimal filtering over lossy networks,” in *Proc. 59th IEEE Conf. Decis. Control (CDC)*, 2020, pp. 4336–4341.
- [10] Y. Feng, X. Nie, and X. Chen, “Multi-objective filtering for discrete-time systems in the presence of data packet drops,” in *Proc. 57th IEEE Conf. Decis. Control (CDC)*, 2018, pp. 2297–2302.
- [11] H. Wang, H. Li, J. Fang, and H. Wang, “Robust Gaussian Kalman filter with outlier detection,” *IEEE Signal Process. Lett.*, vol. 25, no. 8, pp. 1236–1240, Aug. 2018.
- [12] N. Ma, H. Zhang, H. Hu, and Y. Qin, “ESCVAD: An energy-saving routing protocol based on Voronoi adaptive clustering for wireless sensor networks,” *IEEE Internet Things J.*, vol. 9, no. 11, pp. 9071–9085, Jun. 2022.
- [13] W. Vijitkunsawat and P. Anunvrapong, “Multi-adaptive routing protocol for vehicular ad hoc network,” in *Proc. Int. Conf. Digit. Inf. Commun. Technol. Appl. (DICTAP)*, 2012, pp. 359–362.
- [14] A. T. Fisch, I. A. Eckley, and P. Fearhead, “Innovative and additive outlier robust Kalman filtering with a robust particle filter,” *IEEE Trans. Signal Process.*, vol. 70, pp. 47–56, 2021.
- [15] O. S. Chernikova, “An adaptive unscented Kalman filter approach for state estimation of nonlinear continuous-discrete system,” in *Proc. Int. Sci. Tech. Conf. Actual Probl. Electron. Instrum. Eng. (APEIE)*, 2018, pp. 37–40.
- [16] H. Wang, D. Liu, T. Chen, and X. Qin, “A robust state estimation method for unknown, time-varying and featureless aircraft sensor failures,” *IEEE Access*, vol. 8, pp. 118125–118134, 2020.
- [17] H. Fang, M. A. Haile, and Y. Wang, “Robust extended Kalman filtering for systems with measurement outliers,” *IEEE Trans. Control Syst. Technol.*, vol. 30, no. 2, pp. 795–802, Mar. 2022.
- [18] C. Bilen, G. Puy, R. Gribonval, and L. Daudet, “Convex optimization approaches for blind sensor calibration using sparsity,” *IEEE Trans. Signal Process.*, vol. 62, no. 18, pp. 4847–4856, Sep. 2014.
- [19] Q. Liu, Z. Wang, X. He, and D. Zhou, “On Kalman-consensus filtering with random link failures over sensor networks,” *IEEE Trans. Autom. Control*, vol. 63, no. 8, pp. 2701–2708, Aug. 2018.
- [20] S. Battilotti, F. Cacace, M. d’Angelo, and A. Germani, “Distributed kalman filtering over sensor networks with unknown random link failures,” *IEEE Control Syst. Lett.*, vol. 2, no. 4, pp. 587–592, Oct. 2018.
- [21] L. Paradis and Q. Han, “A survey of fault management in wireless sensor networks,” *J. Netw. Syst. Manag.*, vol. 15, no. 2, pp. 171–190, 2007.
- [22] C. Yang, J. Zheng, X. Ren, W. Yang, H. Shi, and L. Shi, “Multi-sensor Kalman filtering with intermittent measurements,” *IEEE Trans. Autom. Control*, vol. 63, no. 3, pp. 797–804, Mar. 2018.
- [23] T. Nie, Z. Deng, Y. Wang, and X. Qin, “A robust unscented Kalman filter for intermittent and featureless aircraft sensor faults,” *IEEE Access*, vol. 9, pp. 28832–28841, 2021.
- [24] J. Zhang, K. You, and L. Xie, “Bayesian filtering with unknown sensor measurement losses,” *IEEE Trans. Control Netw. Syst.*, vol. 6, no. 1, pp. 163–175, May 2019.
- [25] A. N. Alvi et al., “OGMAD: Optimal GTS-allocation mechanism for adaptive data requirements in IEEE 802.15.4 based Internet of Things,” *IEEE Access*, vol. 7, pp. 170629–170639, 2019.
- [26] A. Faridi et al., “Comprehensive evaluation of the IEEE 802.15.4 MAC layer performance with retransmissions,” *IEEE Trans. Veh. Technol.*, vol. 59, no. 8, pp. 3917–3932, Oct. 2010.
- [27] G. Chen, X. Cao, and J. Jin, “Joint scheduling and channel allocation for Kalman filtering over multihop WirelessHART networks,” *IEEE Trans. Ind. Informat.*, vol. 17, no. 5, pp. 3555–3565, May 2021.
- [28] M. Sha, D. Gunatilaka, C. Wu, and C. Lu, “Empirical study and enhancements of industrial wireless sensor–actuator network protocols,” *IEEE Internet Things J.*, vol. 4, no. 3, pp. 696–704, Jun. 2017.
- [29] F. Dobslaw, T. Zhang, and M. Gidlund, “End-to-end reliability-aware scheduling for wireless sensor networks,” *IEEE Trans. Ind. Informat.*, vol. 12, no. 2, pp. 758–767, Apr. 2016.
- [30] Z. Yemeni, H. Wang, W. M. Ismael, A. Hawbani, and Z. Chen, “CFDDR: A centralized faulty data detection and recovery approach for WSN with faults identification,” *IEEE Syst. J.*, vol. 16, no. 2, pp. 3001–3012, Jun. 2022.

- [31] K. P. Sharma and T. P. Sharma, "rDFD: Reactive distributed fault detection in wireless sensor networks," *Wireless Netw.*, vol. 23, pp. 1145–1160, May 2017.
- [32] B. Li, L. Nie, C. Wu, H. Gonzalez, and C. Lu, "Incorporating emergency alarms in reliable wireless process control," in *Proc. 6th ACM/IEEE Int. Conf. Cyber Phys. Syst.*, 2015, pp. 218–227.
- [33] Y. Ma, D. Gunatilaka, B. Li, H. Gonzalez, and C. Lu, "Holistic cyber-physical management for dependable wireless control systems," *ACM Trans. Cyber Phys. Syst.*, vol. 3, no. 1, pp. 1–25, 2018.
- [34] Y. Li, D. E. Quevedo, V. Lau, and L. Shi, "Multi-sensor transmission power scheduling for remote state estimation under SINR model," in *Proc. 53rd IEEE Conf. Decis. Control (CDC)*, 2014, pp. 1055–1060.
- [35] K. Ding, Y. Li, D. E. Quevedo, S. Dey, and L. Shi, "A multi-channel transmission schedule for remote state estimation under DoS attacks," *Automatica*, vol. 78, pp. 194–201, Apr. 2017.
- [36] H. Ma, L. Wang, and S. Zhou, "Scheduling to minimize control cost in multi-loop wireless networked control with imperfect sensors," in *Proc. IEEE 95th Veh. Technol. Conf. (VTC-Spring)*, 2022, pp. 1–7.
- [37] O. Ayan, M. Vilgelm, M. Klügel, S. Hirche, and W. Kellerer, "Age-of-information vs. value-of-information scheduling for cellular networked control systems," in *Proc. 10th ACM/IEEE Int. Conf. Cyber Phys. Syst.*, 2019, pp. 109–117.
- [38] E. Henriksson, D. E. Quevedo, E. G. Peters, H. Sandberg, and K. H. Johansson, "Multiple-loop self-triggered model predictive control for network scheduling and control," *IEEE Trans. Control Syst. Technol.*, vol. 23, no. 6, pp. 2167–2181, Nov. 2015.
- [39] D. Bernardini and A. Bemporad, "Energy-aware robust model predictive control based on noisy wireless sensors," *Automatica*, vol. 48, no. 1, pp. 36–44, 2012.
- [40] B. Sinopoli, L. Schenato, M. Franceschetti, K. Poolla, M. I. Jordan, and S. S. Sastry, "Kalman filtering with intermittent observations," *IEEE Trans. Autom. Control*, vol. 49, no. 9, pp. 1453–1464, Sep. 2004.
- [41] S. He, H.-S. Shin, S. Xu, and A. Tsourdos, "Distributed estimation over a low-cost sensor network: A review of state-of-the-art," *Inf. Fusion*, vol. 54, pp. 21–43, Feb. 2020.
- [42] F. Group. "WirelessHART." Accessed: Nov. 11, 2022. [Online]. Available: <https://fieldcommgroup.org/technologies/hart/hart-technology>
- [43] K. Zhou, J. Doyle, and K. Glover, "Robust and optimal control," *Control Eng. Pract.*, vol. 4, no. 8, pp. 1189–1190, 1996.
- [44] W. Liu, G. Nair, Y. Li, D. Nescic, B. Vucetic, and H. V. Poor, "On the latency, rate, and reliability tradeoff in wireless networked control systems for IIoT," *IEEE Internet Things J.*, vol. 8, no. 2, pp. 723–733, Jan. 2021.
- [45] W. Liu, P. Popovski, Y. Li, and B. Vucetic, "Wireless networked control systems with coding-free data transmission for industrial IoT," *IEEE Internet Things J.*, vol. 7, no. 3, pp. 1788–1801, Mar. 2020.
- [46] Y. Mo and B. Sinopoli, "Kalman filtering with intermittent observations: Tail distribution and critical value," *IEEE Trans. Autom. Control*, vol. 57, no. 3, pp. 677–689, Sep. 2011.
- [47] V. Shilpiekandula, S. A. Bortoff, J. C. Barnwell, and K. El Rifai, "Load positioning in the presence of base vibrations," in *Proc. Amer. Control Conf. (ACC)*, 2012, pp. 6282–6287.
- [48] Y. Ma et al., "Optimal dynamic transmission scheduling for wireless networked control systems," *IEEE Trans. Control Syst. Technol.*, vol. 30, no. 6, pp. 2360–2376, 2022.
- [49] J. Song et al., "WirelessHART: Applying wireless technology in real-time industrial process control," in *Proc. IEEE Real Time Embedded Technol. Appl. Symp.*, 2008, pp. 377–386.
- [50] A. H. Chughtai, M. Tahir, and M. Uppal, "Outlier-robust filtering for nonlinear systems with selective observations rejection," *IEEE Sens. J.*, vol. 22, no. 7, pp. 6887–6897, 2022.
- [51] H.-Q. Mu and K.-V. Yuen, "Novel outlier-resistant extended Kalman filter for robust online structural identification," *J. Eng. Mech.*, vol. 141, no. 1, 2015, Art. no. 4014100.
- [52] D. De Palma and G. Indiveri, "Output outlier robust state estimation," *Int. J. Adapt. Control Signal Process.*, vol. 31, no. 4, pp. 581–607, 2017.
- [53] M. Panda and P. M. Khilar, "Distributed self fault diagnosis algorithm for large scale wireless sensor networks using modified three sigma edit test," *Ad Hoc Netw.*, vol. 25, pp. 170–184, Feb. 2015.
- [54] V. P. Bhuvana, C. Preissl, A. M. Tonello, and M. Huemer, "Multi-sensor information filtering with information-based sensor selection and outlier rejection," *IEEE Sensors J.*, vol. 18, no. 6, pp. 2442–2452, Mar. 2018.
- [55] X. Kong, X. Zhang, N. Lu, Y. Ma, and Y. Li, "Online smart meter measurement error estimation based on EKF and LMRLS method," *IEEE Trans. Smart Grid*, vol. 12, no. 5, pp. 4269–4279, Sep. 2021.
- [56] M. Eisen, M. M. Rashid, K. Gatsis, D. Cavalcanti, N. Himayat, and A. Ribeiro, "Control aware radio resource allocation in low latency wireless control systems," *IEEE Internet Things J.*, vol. 6, no. 5, pp. 7878–7890, Oct. 2019.
- [57] C. Wu, D. Gunatilaka, M. Sha, and C. Lu, "Real-time wireless routing for Industrial Internet of Things," in *Proc. IEEE/ACM 3rd Int. Conf. Internet Things Design Implement. (IoTDI)*, 2018, pp. 261–266.
- [58] D. Q. Mayne, J. B. Rawlings, C. V. Rao, and P. O. Scokaert, "Constrained model predictive control: Stability and optimality," *Automatica*, vol. 36, no. 6, pp. 789–814, 2000.
- [59] F. Mager, D. Baumann, R. Jacob, L. Thiele, S. Trimpe, and M. Zimmerling, "Feedback control goes wireless: Guaranteed stability over low-power multi-hop networks," in *Proc. 10th ACM/IEEE Int. Conf. Cyber Phys. Syst.*, 2019, pp. 97–108.
- [60] D. Baumann, F. Mager, R. Jacob, L. Thiele, M. Zimmerling, and S. Trimpe, "Fast feedback control over multi-hop wireless networks with mode changes and stability guarantees," *ACM Trans. Cyber Phys. Syst.*, vol. 4, no. 2, pp. 1–32, 2019.



Ruijie Fu received the B.S. degree in automatic control from Jilin University, Changchun, China, in 2022. He is currently pursuing the Ph.D. degree with the School of Electronic Information and Electrical Engineering, Shanghai Jiao Tong University, Shanghai, China.

His current research interests include the co-design of control and scheduling in industrial cyber-physical systems, and Industrial Internet of Things.



Jintao Chen received the B.S. degree in automatic control from Shanghai Jiao Tong University, Shanghai, China, in 2023, where he is currently pursuing the Ph.D. degree with the School of Electronic Information and Electrical Engineering.

His current research interests include real-time scheduling, real-time control, and intelligent control.



Yutong Lin received the B.S. degree in automatic control from Shanghai Jiao Tong University, Shanghai, China, in 2023, where he is currently pursuing the M.S. degree with the school of Electronic Information and Electrical Engineering.

His current research interests include multisensor fusion for robot navigation and multiagent systems.



An Zou (Member, IEEE) received the B.S. and M.S. degrees from Harbin Institute of Technology, Harbin, China, in 2013 and 2015, respectively, and the Ph.D. degree in electrical engineering from Washington University, St. Louis, MO, USA, in 2021.

He is an Assistant Professor with the University of Michigan-Shanghai Jiao Tong University Joint Institute, Shanghai Jiao Tong University, Shanghai, China. His work has been extensively published and recognized at top-tier conferences and journals, including *Micro*, *DAC*, *ICCAD*, *IEEE TRANSACTIONS ON COMPUTER-AIDED DESIGN OF INTEGRATED CIRCUITS AND SYSTEMS*, *ACM Transactions on Architecture and Code Optimization*, and *RTAS*. His research focuses on computer architecture and embedded systems.



Cailian Chen (Member, IEEE) received the B.Eng. and M.Eng. degrees in automatic control from Yanshan University, Qinhuangdao, China, in 2000 and 2002, respectively, and the Ph.D. degree in control and systems from The City University of Hong Kong, Hong Kong, in 2006.

She is currently a Full Professor with the Department of Automation, Shanghai Jiao Tong University, Shanghai, China. Her research interests include industrial wireless networks and computational intelligence, and Internet of Vehicles.

Prof. Chen was honored the Outstanding Young Researcher by NSF of China in 2020 and the Changjiang Young Scholar in 2015. She serves as an Associate Editor of IEEE TRANSACTIONS ON VEHICULAR TECHNOLOGY, IET Cyber-Physical Systems: Theory and Applications, Peer-to-peer Networking and Applications (Springer). She also served as the Guest Editor of IEEE TRANSACTIONS ON VEHICULAR TECHNOLOGY, a TPC Chair of ISAS19, a Symposium TPC Co-Chair of IEEE Globecom 2016, a Track Co-Chair of VTC2016-Fall and VTC2020-Fall, and a Workshop Co-Chair of WiOpt18.



Yehan Ma (Member, IEEE) received the B.S. and M.S. degrees from Harbin Institute of Technology, Harbin, China, in 2013 and 2015, respectively, and the Ph.D. degree in computer science from Washington University in St. Louis, St. Louis, MO, USA, in 2020.

She is an Assistant Professor with the School of Electronic Information and Electrical Engineering, Shanghai Jiao Tong University, Shanghai, China. She broadly investigated techniques and solutions for holistic managements of computation, communication, and control in cyber-physical systems. Her work has been published at top-tier conferences and journals, such as EMSOFT, ICCPS, and IEEE TRANSACTIONS ON COMPUTER-AIDED DESIGN OF INTEGRATED CIRCUITS AND SYSTEMS. Her research focuses on the Industrial Internet of Things, cyber-physical systems, and edge computing.

Dr. Ma serves as the TPC of RTSS, SECON, and ECRTS.



Xiping Guan (Fellow, IEEE) received the B.Sc. degree in mathematics from Harbin Normal University, Harbin, China, in 1986, and the Ph.D. degree in control science and engineering from Harbin Institute of Technology, Harbin, in 1999.

He is the Chair Professor with Shanghai Jiao Tong University, Shanghai, China, where he is the Dean of the School of Electronic, Information and Electrical Engineering and the Director of the Key Laboratory of Systems Control and Information Processing, Ministry of Education of China. He has authored or coauthored five research monographs, more than 200 papers in IEEE transactions, other peer-reviewed journals, and numerous conference papers. His current research interests include industrial network systems, smart manufacturing, and underwater networks.

Prof. Guan is a National Outstanding Youth honored by NSF of China, the Changjiang Scholar's by the Ministry of Education of China, and the State-Level Scholar of New Century Bai Qianwan Talent Program of China. He is an Executive Committee Member of Chinese Automation Association Council and the Chinese Artificial Intelligence Association Council.